Green Chemistry

TUTORIAL REVIEW

View Article Online
View Journal | View Issue

Cite this: *Green Chem.*, 2023, **25**, 3816

Waste to wealth: direct utilization of spent materials for electrocatalysis and energy storage

Chengcheng Yan,†[a] Xun Jiang,†[a] Jiaxin Yu,[a] Zhaolong Ding,[a] Ling Ma,[a] Tingyu Su,[a] Yilu Wang,[a] Chunxia Wang, *[a] Guoyong Huang *[a] and Shengming Xu [b]

The pursuit of carbon neutrality in today's world has led to the development of environmentally friendly, sustainable energy sources. The conversion of waste into wealth in electrocatalysis and energy conversion and storage not only mitigates environmental pressure but also provides valuable electrode materials for the energy crisis with comprehensive economic benefits. Herein, a comprehensive review of the recent advances in transforming spent materials into highly active species in energy related fields is presented, focusing on versatile waste sources, synthetic strategies, structural properties, electrochemical performances, and applications in clean sustainable energy fields. Firstly, we provide a brief description and discussion of the synthetic methods employed in the transformation of waste. Secondly, waste materials containing precious metals, carbon sources, heteroatoms, and interlinked structures that are treated using different synthetic strategies for reutilization in various electrocatalysis are systematically discussed. Thirdly, by taking full advantage of the rich porosity, high surface area, multiple electron transport channel and high conductivity, these spent materials are substantially employed as highly efficient materials in energy conversion and storage systems which are classified into various types of batteries and supercapacitors. Finally, the challenges and prospects for green and sustainable resources in the burgeoning field of waste to wealth utilization in energy conversion and storage are proposed.

Received 29th January 2023,
Accepted 18th April 2023

DOI: 10.1039/d3gc00323j

rsc.li/greenchem

1. Introduction

The pursuit of clean renewable energy sources has stimulated the growing demand for energy materials. Electrocatalytic reactions involving the hydrogen evolution reaction (HER), the oxygen evolution reaction (OER), the oxygen reduction reaction (ORR), the carbon dioxide reduction reaction (CO_2RR) and the nitrogen reduction reaction (NRR) are important chemical

[a]*State Key Laboratory of Heavy Oil Processing, College of New Energy and Materials, China University of Petroleum (Beijing), Beijing 102249, China.*
E-mail: cxwang@iccas.ac.cn, huanggy@cup.edu.cn
[b]*Beijing Key Lab of Fine Ceramics, Institute of Nuclear and New Energy Technology, Tsinghua University, Beijing, 100084, China*
†These authors contributed equally.

Chengcheng Yan

Chengcheng Yan received his Bachelor's Degree from Henan University of Technology in China in 2021. He is currently a Master's student at China University of Petroleum (Beijing). His research interests focus on the utilization of recycled resources for electrocatalysis and energy storage.

Xun Jiang

Xun Jiang is an undergraduate student in New Energy of Science and Engineering at China University of Petroleum (Beijing). Her research interests are the development of renewable resource derived nanomaterials in the field of energy storage.

conversion processes for the production of clean sustainable energy.[1–3] More importantly, various secondary rechargeable batteries including lithium-ion batteries (LIBs), lithium–sulfur batteries (LSBs), lithium–oxygen batteries (LOBs), sodium-ion batteries (SIBs), potassium-ion batteries (KIBs), zinc-ion batteries (ZIBs), zinc–air batteries (ZABs), and supercapacitors also play a crucial role in electrochemical energy storage systems.[4–7] Notably, the key substances for electrocatalysis and energy conversion and storage systems rely heavily on active precious metals, valuable transition metals and diverse structure substrate materials. The prices of all these materials have risen dramatically over the past decade, and therefore it is necessary to identify widely available highly efficient electrocatalysts and key electrode materials that are suitable for low-cost production.[8] Due to the ever-growing consumption of natural resources and the huge production of waste, transforming waste that contains abundant renewable resources into wealth has aroused tremendous attention.[9] Differing from the traditional waste disposal methods through dumping, or burning, rational direct conversion of waste into electrocatalysts and important electrode materials could minimize waste emissions and pollution problems as well as improve resource utilization.[10,11]

Recently, extensive research has been devoted to exploring the direct conversion of a wide range of waste containing rich valuable metals and elements through reasonable chemical and physical treatment.[12–14] Spent batteries are rich in active metals (Li, Ni, Co and Mn) which can be selectively utilized as active sites for electrocatalysts and electrode materials in energy storage systems.[15,16] Waste graphite in spent batteries can be used as substrates for electrocatalysts and electrode materials in energy storage systems after treatment or complexing with other materials.[17–19] Biomass features diverse morphologies and heteroatoms serve as an ideal source for the production of different dimentional carbonaceou materials through hydrothermal and carbonization processes with the assistance of activation.[20–22] Therefore, naturally abundant biomass-derived carbonaceous materials are widely used as carrier materials due to their tunable porosity, rich surface chemistry, and fast ion/electron transport.[23,24] In addition, valuable metals and substances in municipal sludge, waste plastics and spent catalysts can be used to prepare various electrocatalysts and electrode materials through leaching, electrochemical deposition, and hydrothermal and other means.[25,26] Moreover, municipal sludge contains a large number of organic compounds and a rich source of carbon, which can be used as a carbon skeleton for the preparation of self-doped heteroatom electrocatalysts.[27,28] Plastic mainly consists of polymers that can be used as available carbon precursors for the manufacture of carbon substrate of electrocatalyst in a cost-effective manner.[29,30] Even industrial waste materials such as copper in waste wire, steel wire in waste tires, silicon in waste photovoltaic materials, various metals in waste circuit boards, and valuable metals and elements in solid or liquid wastes contribute to a large market prospect for reutilization.[25,31–33]

To date, a few reviews have been published on the utilization of biomass derived electrocatalysts in energy storage that focus on the synthetic strategies and functionalization.[7,34,35] A review was recently published on the design of electrocatalysts from waste and natural materials.[36] Some reviews mainly focus on the metal recovery process of waste in an industrial field.[8,9] The direct preparation of key materials in both electrocatalysis and energy storage from comprehensive waste materials such as waste batteries, biomass, municipal sludge, plastics, electronic waste, spent catalysts, and other wastes remains challenging.

Herein, we aim to provide a comprehensive review based on the direct use of waste in electrocatalysis (HER, OER, ORR, CO_2RR and NRR) and energy storage (LIBs, LSBs, LOBs, SIBs, KIBs, ZIBs, ZABs and supercapacitors) with emphasis on versatile waste sources, synthetic strategies as well as the electrochemical performance, as shown in Fig. 1. Firstly, we summarize and discuss the advantages and disadvantages of various methods including calcination, hydrothermal, wet chemical and ball milling methods for the conversion of waste to valuable materials in electrocatalysis and energy storage. Secondly, we systematically review the current advancement of direct

Jiaxin Yu

JiaXing Yu is an undergraduate student in New Energy Science and Engineering at China University of Petroleum (Beijing). Her research interests are the preparation of non-precious metal nanomaterials and their applications in water splitting.

Ling Ma

Ling Ma received her Bachelor's Degree from Xi'an Shiyou University in China in 2022. She is currently a Master's student at China University of Petroleum (Beijing). Her research interests focus on the design and synthesis of new kinds of electrocatalysts and electrode materials.

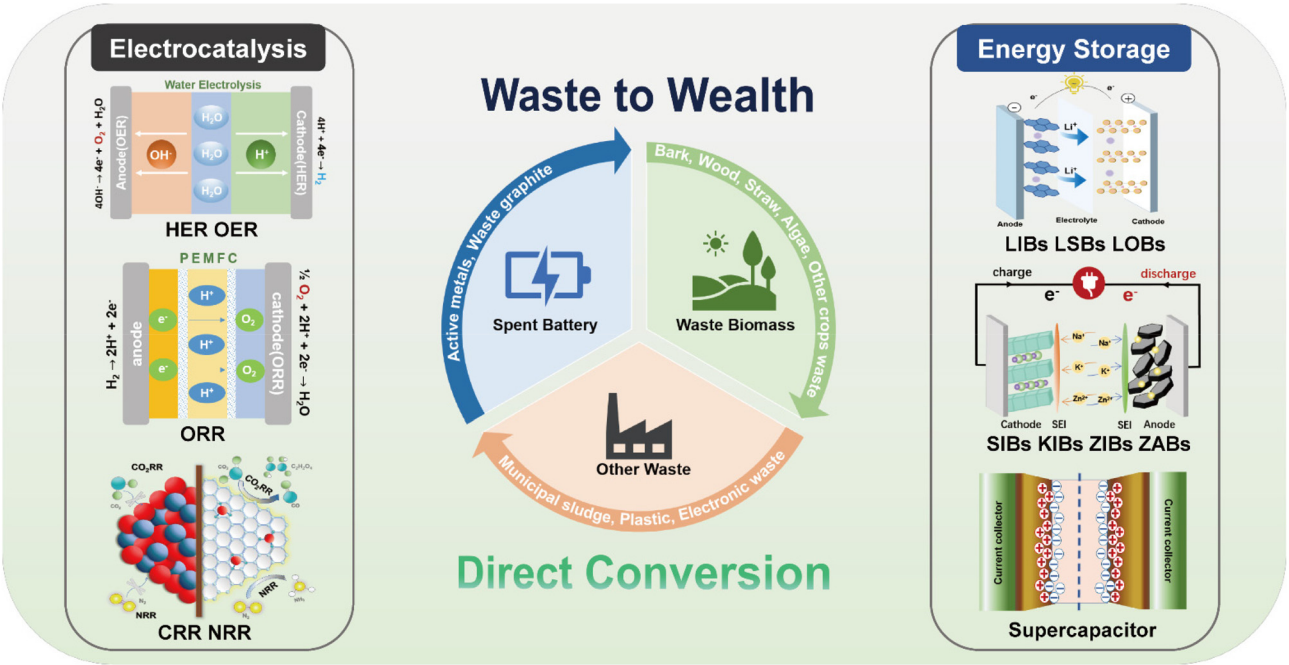

Fig. 1 Schematic illustration of the direct conversion of waste for electrocatalysis and energy storage.

utilization of waste in electrocatalysis, emphasizing on the synthetic procedure and electrochemical performance by using waste batteries, biomass, e-waste, plastics and municipal sludge containing various valuable species. Thirdly, we describe the synthetic strategies and electrochemical properties of various electrode materials for energy storage devices derived from waste batteries, biomass and silicon containing waste (photovoltaic materials, waste glass). Finally, the challenges and prospects of transforming versatile waste materials into clean sustainable energy are summarized. This review summarizes the direct utilization of waste as key materials for electrocatalysts and energy storage systems from green and sustainable resources, which accelerates the development of clean energy and prompts carbon neutrality.

2. Synthetic methods

Waste materials come from a wide range of sources with different compositions and morphologies. Depending on the active specie, component, structure, and morphology of waste materials, diverse synthetic methods have been developed. This section summarizes the various synthetic methods of direct utilization of waste materials, which is shown in Table 1.

2.1. Calcination method

Calcination method refers to the process of treating solid raw materials at temperatures typically ranging from several hundreds to thousand degrees Celsius under a controlled atmosphere, and this process alters the atomic or molecular struc-

Chunxia Wang

Chunxia Wang is currently an associate professor at the College of New Energy and Materials, China University of Petroleum (Beijing). She received her PhD degree from Tohoku University and pursued postdoctoral studies at the Institute of Chemistry, Chinese Academy of Sciences. Her research interests are the development of functional low-dimensional nanomaterials and their application in electrocatalysis and energy related fields.

Guoyong Huang

Guoyong Huang received his BS (2005) in Polymer Science and Engineering, MS (2007) and PhD (2015) in Chemical Engineering and Technology from Tsinghua University in China. In 2019, he became a professor at the College of New Energy and Materials at China University of Petroleum, Beijing. His research is devoted to the utilization of recycled resources in clean energy.

Table 1 Synthetic methods for the conversion of waste to wealth.

Method	Waste source	Available material	New material	Application
Calcination	Spent battery	Graphite, Co, Fe, Ni, Mn	Mn_3O_4 [81]	OER
			CoFe/C,[110] $Li(Ni_{1/3}CO_{1/3}Mn_{1/3})O_2$ [153]	ORR
			TRGNs-MoS_2 [215]	LIBs
				Supercapacitors
	Biomass	Corn stover[49]	Porous activated carbon	HER
		Onion peels[93]		OER
		Red dates[114]		ORR
		Tobacco stems[115]		CO_2RR
		Reed[173]		LIBs
		Apples[195]		LOBs
		Nori[185]		LSBs
		Wood sawdust[197]		SIBs
		Bagasse[201]		KIBs
	Plastic	PET[63]	Activated carbon	HER
		PE[118]		ORR
		PU[120]		LSBs
		PS[229]		Supercapacitors
	Sludge	Municipal sludge[28,142]	Porous carbon	CO_2RR
		Electroplating sludge[143]	$CuCr_2O_4$	NRR
	Worn-out tires	Stainless steel wires[31]	$MoNi_4$/SSW	HER
	Waste catalyst	Ni[99]	NAlCNTs-c50	OER
	Industrial waste	Glass microfiber filter[164]	Si NPs	LIBs
		Engine oil[231]	Porous activated carbon	Supercapacitors
Hydrothermal	LIBs	Mn, Co	$MnCo_2O_4$ [210]	Supercapacitors
	Biomass	Babassu coconut[133]	Ag@C	CO_2RR
		Waste corn stover[219]	CNR/HTC/CFs	Supercapacitors
	Waste catalyst	Graphitic carbon[98]	MoS_2@GC	OER
		V[205]	$V_{10}O_{22.8}\cdot 12H_2O$	ZIBs
	Plastic	PET[61]	ZnO@NMC	HER
	Sludge	Digested sludge[135]	NPC	CO_2RR
Wet-chemical	Spent battery	$LiFePO_4$ [78]	Ni-$LiFePO_2$	OER
		$LiNi_{0.6}Co_{0.2}Mn_{0.2}O_2$ [155]	$LiNi_{0.6}Co_{0.2}Mn_{0.2}O_2$	LIBs
		$LiNi_{1-x-y}Mn_xCo_yO_2$ [206]	NiMnCo-AC	ZABs
	Scrap copper wires	Cu[25]	NiCoP/SCW	HER
	Cu–Sn bronze	Cu, Sn[127]	$Cu_{10}Sn$	CO_2RR
	Waste catalyst	$CaSi_2$ [226]	Siloxene sheets	Supercapacitors
Ball milling	Spent battery	Graphite[13]	Functional interlayer	LSBs
	Circuit boards	Cu, Sn, Fe, Al, Ag, Ni[128]	Ultrafine/nanocrystalline powder	CO_2RR
	Industrial waste	Si[167]	Si/CNTs/C	LIBs

tural changes that in turn affect their physical and chemical properties. The calcination method can quickly process large amounts of waste by extracting metals such as nickel, cobalt, iron, and lithium, which were then used in electrocatalysis and secondary batteries. By adjusting the calcination temperature, time, and atmosphere, biomass, plastics, and sludge containing the organic substancescan be completely decomposed, achieving precise control of the porosity and surface area of the carbon material.[11,35] However, the calcination method not only requires a large amount of energy consumption but also produces harmful gases and undesired impurities, which can lead to impure carbon materials and requires additional treatment for purification.[28]

2.2. Hydrothermal method

The hydrothermal method features with the synthesis of nanomaterials in aqueous solutions or organic solvents at moderate temperatures in an autoclave. The enhanced activity of water (or organic solvent) molecules under high temperature and pressure conditions can promote the chemical reaction. It can be used to prepare fine powders with small particle size, uniform distribution, and complete crystal grain by adjusting the reaction conditions without producing harmful gases or pollutants.[61] Hydrothermal method is widely used in the fields of recycling waste batteries, biomass, plastics, and sludge. However, the reaction yield is comparatively low owing to the high pressure and extended reaction time.

2.3. Wet-chemical method

The wet-chemical method is performed based on chemical reactions including acid–base leaching, chemical precipitation, and electrochemical deposition under mild conditions. It is usually combined with calcination and ball milling for extraction, separation, or loading of metals from waste.[78] The reaction conditions and chemical reagents greatly affect the utilization efficiency of the active substance. The synthetic method for different waste materials and target substances largely depended on the use of strong acids and bases, which complicate the post-treatment procedure and exert large pressure on the environment.

2.4. Ball milling method

The ball milling method utilizes the high-speed rotation of a ball mill to drive the rotating cylinder, while the grinding balls

inside the cylinder collide, shear, and friction with the materials, enabling the formation of the material's crystal structure and surface chemistry, which can be used for large-scale production in an environmentally friendly manner.[128] Compared with the calcination method, hydrothermal method, and wet chemical method, ball milling results in a wider particle size distribution (nanometer to micrometer range) and longer preparation time. The ball milling method may not be applicable for waste materials with unstable chemical components, since the active species will lose activity.[13]

3. Waste to wealth in electrocatalysis

Electrocatalysts used in the HER, OER, ORR, CO_2RR, and NRR typically require noble and transition metals such as Pt, Ru, Co, Ni, Cu and Fe as active components, to enhance the activity and selectivity of electrochemical reaction. For example, Pt, Ru, Ni, Co and Fe in waste materials show suitable adsorption energy for hydrogen and oxygen, which is particularly suitable for the HER, OER and ORR.[14,25,52] The Cu in the waste material has moderate binding energy for key reaction intermediates during the electroreduction of CO_2 and N_2.[33,143] In addition, carbon-containing waste materials such as biomass, sludge, and plastics can be converted into carbon materials with large specific surface area and rich pore channels, providing sufficient catalytic sites and ion transport channels.[28,49,63] This part reviews the application progress of versatile types of waste materials in the field of the HER, OER, ORR, CO_2RR, and NRR.

3.1. Hydrogen evolution reaction (HER)

Electrochemical water splitting has been proven to be a promising route to produce H_2.[37] Pt, Ru, and Pd are ideal electrocatalysts for water splitting. However, their high cost and scarcity hinder large-scale production.[38] Metals in waste (such as nickel, cobalt, and manganese) if not used will cause severe environmental pollution.[39] Thus, the conversion of waste to electrocatalyst has attracted much attention in emerging renewable energy technologies.[8] This section provides an overview of eco-designed HER catalysts and highlights representative strategies.

Electronic waste for HER electrocatalysts. Engineering HER electrocatalysts from electronic-waste and spent LIBs has been extensively investigated by using various approaches. As shown in Fig. 2A, by using scrap copper wires (SCWs), nickel cobalt phosphide (NiCoP), a bifunctional electrocatalyst can be prepared through a simple electrodeposition approach. Due to the close electrical connection between NiCoP and copper wires, fast mass transport and enhanced charge transfer can be expected, synergistically providing an integrated nonnoble electrocatalyst with an overpotential of 178 mV at 10 mA cm^{-2} in KOH solution.[25] Many spent LIBs normally contain rich Ni, Co, and Mn, which can be regarded as valuable metals and recovered for further utilization. For example, Liu *et al.* utilized Co from spent LIBs to synthesize a three-dimensional sea urchin-type cobalt nitride bifunctional electrocatalyst (CoN-Gr-2) through a hydrothermal process (Fig. 2B). Benefiting from the high conductivity, large specific surface area and sea-urchin-like structure, CoN-Gr-2 exhibits exposed active sites, superior mass transfer and electron transfer efficiency, delie-

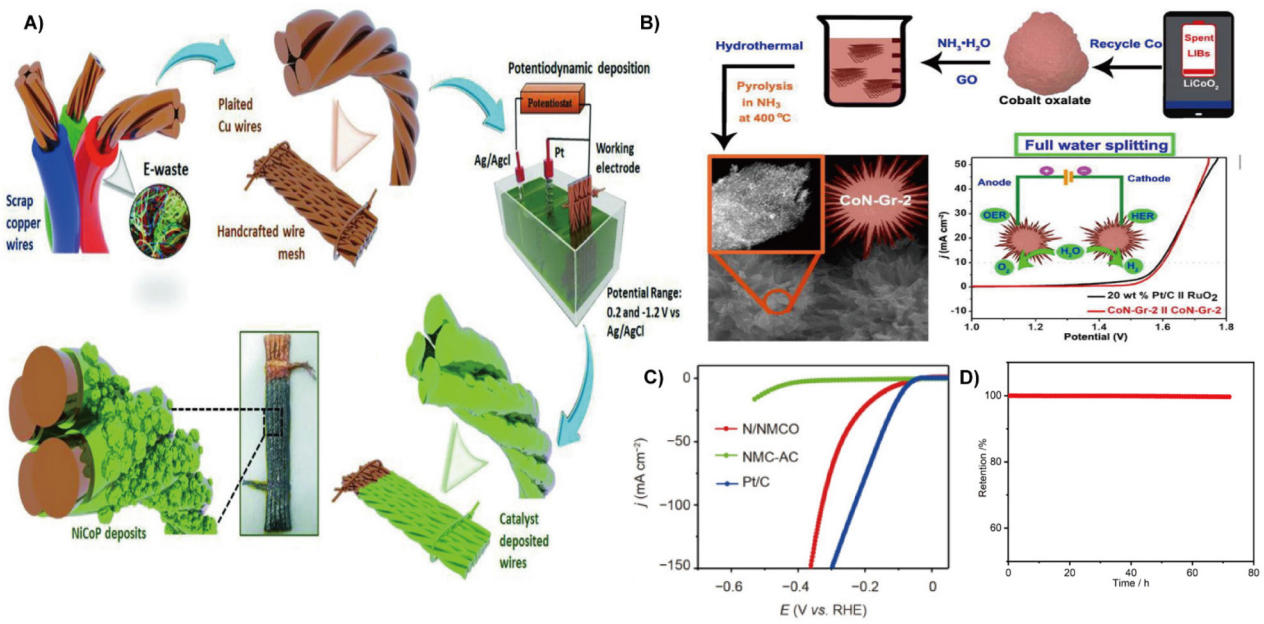

Fig. 2 (A) Schematic illustration of the electrode fabrication from scrap copper wires.[25] Reprinted with permission. Copyright 2018, Wiley-VCH. (B) Schematic for the complete processes of recycling Co in LIBs and the controllable preparation of tiny CoN tightly coupled 3D sea-urchin-like CoN-Gr-2.[40] Reprinted with permission. Copyright 2021, Elsevier. (C) HER LSV curves of the N/NMCO, NMC-AC, and Pt/C electrocatalysts. (D) The HER catalytic stability tested at 10 mA cm^{-2}.[41] Reprinted with permission. Copyright 2022, Springer.

vering a low overpotential of 128.9 mV in the HER, comparable to commercial 20 wt% Pt/C.[40] Apart from the hydrothermal process, Zheng *et al.* presented an ultrafast carbothermal shock (CTS) to regenerate cathode materials from spent LIBs into versatile electrocatalysts. The commercial cathode, $LiNi_{0.8}Mn_{0.1}Co_{0.1}O_2$ (NMC), was treated by the CTS process to produce the Ni/Ni–Co–Mn–O_x (N/NMCO) composite. The resulting N/NMCO exhibits a small size distribution and increased number of active sites, which accelerate mass transfer, suggesting a low overpotential of 112 mV for the HER (Fig. 2C). Moreover, N/NMCO exhibits excellent stability with almost no degradation after 70 h (Fig. 2D).[41]

Waste biomass for HER electrocatalysts. As an abundant renewable carbon source, biomass serves as an alternative to expensive commerical available chemicals and materials.[42] In recent years, biomass-derived carbon have attracted much attention because of their low cost, environmental friendliness, and diverse structures.[43,44] Expanding the application of biomass based carbon materials as precious metal substitutes in electrocatalysts is a promising and convenient way.[45] Xiao *et al.* prepared a watermelon peel-derived Mo_2C/C electrocatalyst for HER through a pyrolysis procedure (Fig. 3A). The lignocellulosic carbon fiber of watermelon peels forms a porous structure and tends to expose more active sites, which favours mass transfer and prompts electrochemical performance. Therefore, benefiting from unique pore size and large surface area, the watermelon fabricated Mo_2C/C electrocatalyst exhibits excellent HER performance with an overpotential of 133 mV at 10 mA cm^{-2}.[46]

Moreover, heteroatom doping can promote the electronic environment, increase the electronic conductivity and lower the Gibbs free energy of hydrogen adsorption, thereby boosting the electrocatalytic performance.[47] By using waste silk fabric, a self-supporting nitrogen-doped carbon electrocatalyst with a porous three-dimensional (3D) structure through KCl activation was constructed. It showed an overpotential of 336.33 mV and a Tafel slope of 311 mV dec^{-1} at a current density of 10 mA cm^{-2}, while the unactivated carbon showed an overpotential of 504.66 mV and a Tafel slope of 531 mV dec^{-1}.[48] The doping of metallic elements is also beneficial for improving the performance of the HER electrocatalyst. For example, porous nickel/nickel oxide-nitrogen-doped carbon (Ni/NiO-NC) nanosheet composites were constructed directly from waste corn stalks (CSs) *via* impregnation and calcination strategies (Fig. 3B). The Ni/NiO and N self-doped carbon endow them with an active site, excellent electron/mass transfer, and large specific surface area, and finally contributes to excellent HER activity. The optimal Ni/NiO-NC nanosheets showed an overpotential of 179 mV at 10 mV cm^{-2} and a Tafel slope of 111 mV dec^{-1} in 1.0 M KOH media.[49] Waste carrots containing phosphorus act as carbon precursor to achieve Ni deposition in a sustainable way. The presence of phosphorus and Ni nanoparticles enable a high conductivity and active site, thereby offering HER performance.[50] In addition, pomelo peel (PP) derived porous carbon was also successfully developed as a self-supporting electrocatalyst (Co@PPDC) after incorporation of Co nanoparticles. It showed nearly 100% faradaic efficiency and 1.56 mmol h^{-1} H_2 productivity at 265 mV within 12 h.[51] Hong *et al.* recently reported the nitrogen-doped biomass carbon fiber (NBCF) supported nickel nanoparticle electrocatalyst from natural cattail spikes *via* an *in situ* growth process. Due to the interaction between the distinctive Ni nanoparticles and NBCF microstructure, the Ni–N bonds formed in NBCFs enhanced the corrosion resistance and lowered the electron transfer resistance, thereby boosting the activity and stability of the electrocatalyst.[52] Lotus leaf was also employed as a carbon precursor with the assistance of metal to fabricate large surface area and layered Co/MoO_2@N doped carbon nanosheets (CMO@NC) for the HER.[53]

Graphene, graphene nanocages, or spongy graphene are one of the most promising carbonaceous HER electrocatalysts because of their large porosity, high surface area, and excellent electrical conductivity.[55,56] Biomass derived graphene provides an economical and feasible strategy for the large-scale production of high-quality graphene.[57] Using rice hulls as carbon precursors, corrugated graphene (RH-CG) can be synthesized by KOH activation at 600–700 °C (Fig. 3C). The mesoporous RH-CG with a high graphitization degree demonstrated a low overpotential of 9 mV at 10 mA cm^{-2} (Fig. 3D), a Tafel slope of 31 mV dec^{-1} (Fig. 3E).[54] He *et al.* chose waste grapefruit peels to synthesize nitrogen-doped graphitized carbon substrates (NiFe@NC/NGC) *via* impregnation. When evaluated as HER electrocatalysts in alkaline media, the as-prepared electrocatalyst delivered an overpotential of 190 mV at 20 mA cm^{-2}. The NiFe alloy can transfer electrons, decrease the Gibbs free energy of hydrogen adsorption, and enhance the electrocatalytic activity, resulting in high HER performance.[58] In the above-mentioned studies, biomass-based carbon materials that act as both substrate and active materials in HER due to their structural characteristics and intrinsic activity.[59]

Other wastes for HER electrocatalysts. Waste plastic is one kind of solid wastes that cause environmental pollution. Hence, it is imperative to develop novel approaches to deal with these wastes effectively and transform them into valuable materials.[60] By using waste PET plastic and MOF-5, nitrogen-doped mesoporous carbon functionalized zinc oxide (ZnO@NMC) nanocomposites can be prepared by solvothermal method (Fig. 4A). Carbonization leads to a large and dense cubic collapse of mesoporous structure with a high specific surface area and meso-porosity, which provides enough active sites for enhanced activity of HER in 0.5 M KOH solution (overpotential = 0.39 V (η_{10}), Tafel slope = 108 mV dec^{-1}).[61] Supercritical carbon dioxide (sc-CO_2) features low price, low viscosity, nontoxicity, and simple separation in attaining supercritical conditions that are widely used. In the sc-CO_2 system, polyethylene (PE) wastes degraded to produce CNTs with superior structure at comparatively lower temperature. Finally, the electrocatalyst treated after Pd modification showed an overpotential of 36 mV (Fig. 4B) and a Tafel slope of 43 mV dec^{-1} (Fig. 4C), competing with commercial Pt/C.[62] In addition, combining molybdenum carbide carbon with

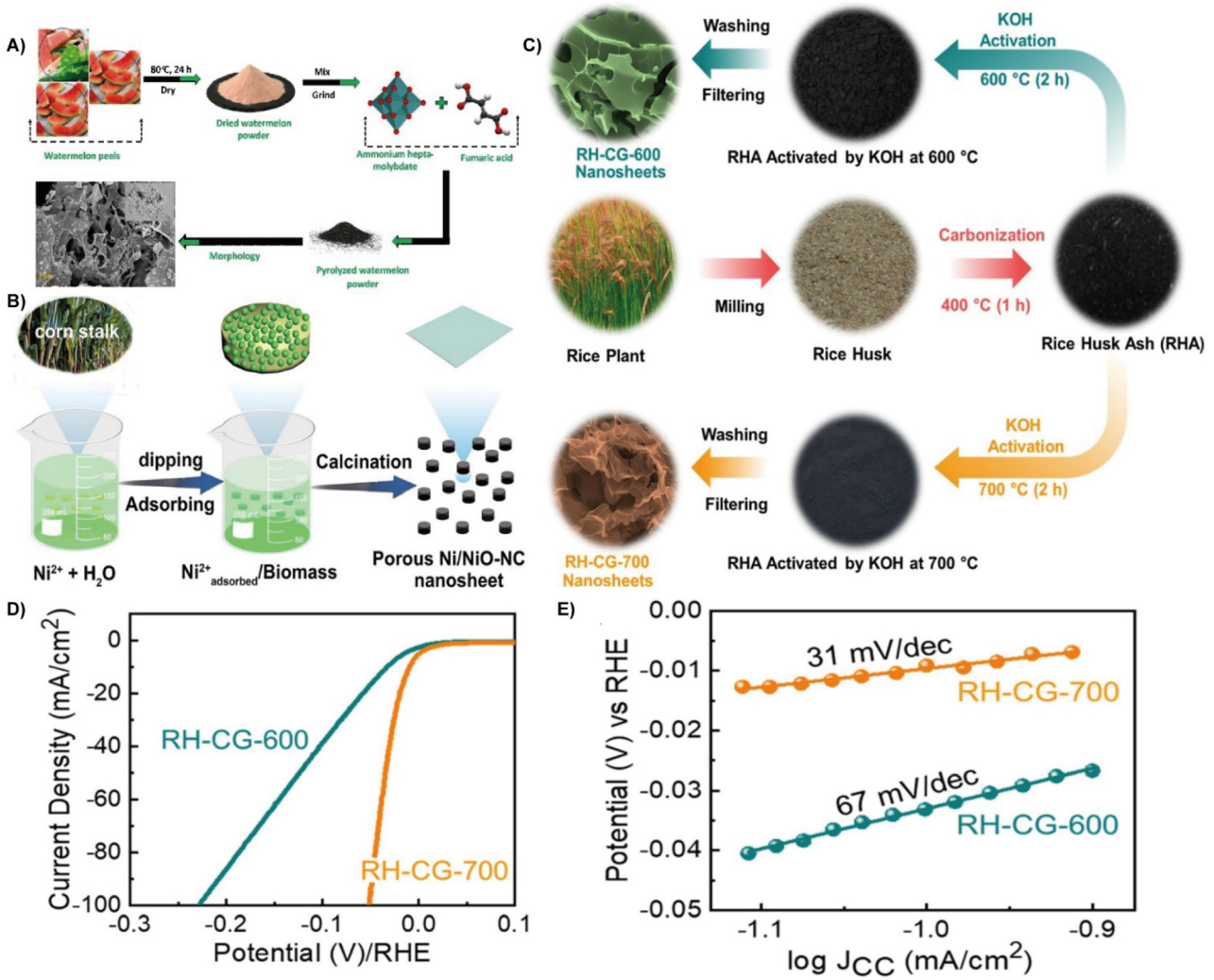

Fig. 3 (A) Schematic illustration of the fabrication process of the prepared electrocatalyst.[46] Reprinted with permission. Copyright 2021, Elsevier. (B) Schematic illustration of the formation of a porous Ni/NiO NC nanosheet composite.[49] Reprinted with permission. Copyright 2022, American Chemical Society. (C) Schematic representation of the experimental procedures for the synthesis of the RH-CG nanosheets *via* the KOH activation method using the biomass red-rice husks. (D) LSV polarization curves for the RH-CG-600 and RH-CG-700 electrodes. (E) Tafel slope curves of the RH-CG-600 and RH-CG-700 electrodes.[54] Reprinted with permission. Copyright 2022, Elsevier.

waste plastic-derived carbon to form carbon nanocomposites (MoC/Mo_2C) can also be used for the HER.[63]

Apart from waste PET plastic, scrap stainless steel wires (SSWs) from damaged tires, cemented carbides and organic liquid waste can also be used to construct HER electrocatalysts. Jothi *et al.* integrated SSWs with highly active $MoNi_4$ to form $MoNi_4$/SSW nanocomposites through thermal decomposition (Fig. 4D), which significantly decreases the energy barrier associated with the Volmer step and accelerates the HER kinetics due to the synergistic effect between Ni and Mo species. Therefore, $MoNi_4$/SSW exhibited remarkable HER performance with a low activation energy (E_a = 16.338 kJ mol^{-1}), low overpotential of 77 mV (200 mA cm^{-2}) and good stability over 150 h.[31] Han *et al.* employed recycled tungsten carbide-cobalt cemented carbides to fabricate a cobalt phosphide (Co_2P) electrocatalyst through a powder metallurgy method. The newly formed Co_2P reduces the activation barrier and reinforces HER performance.[64] In order to reduce the current barrier, organic liquid waste derived vertical graphene nanosheets (VGNSs) were introduced (Fig. 4E). VGNSs are effective in modulating the Schottky barrier contact to increase the HER activity because the heterojunctions possess a low contact resistance and intrinsically good electrical conductivity. The incorporation of MoS_2 into VGNS led to a dramatically reduced energy gap between the Fermi level and the conduction band minimum (CBM) of MoS_2, offering prominent HER activity with a reduction of overpotential by 50 mV and a Tafel slope of 38 mV dec^{-1}.[65] In addition, industrial waste contains large amounts of metals can be used as a metal precursor to form a NiCoMn layered triple hydroxide (LTH) with a hierarchical nanoflower structure by the electrodeposition method. The electrocatalyst exhibited high activity for both OER and HER

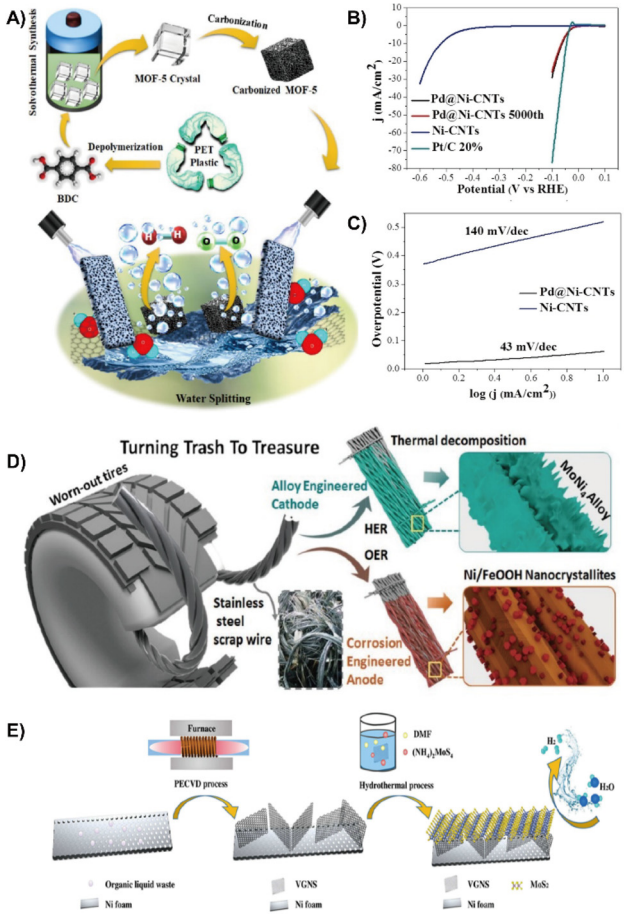

Fig. 4 (A) Reaction scheme for the solovothermal synthesis of ZnO@NMC nanocomposites for HER and OER activity.[61] Reprinted with permission. Copyright 2020, Elsevier. (B) Polarization curves of Pd@Ni-CNTs (7.5 wt%) during the 5000th cycle, and the Ni-CNTs and Pt/C 20% catalyst in a 0.5 M H_2SO_4 electrolyte. (C) the Tafel plots of Pd@Ni-CNTs and Ni-CNTs.[62] Reprinted with permission. Copyright 2018, Wiley-VCH. (D) Schematic illustration showing the fabrication of electrodes for the HER and OER from scrap stainless steel wires (SSWs) derived from worn-out tires.[31] Reprinted with permission. Copyright 2020, Wiley-VCH. (E) Schematic illustration for the synthesis of VGNS and VGNS/MoS_2.[65] Reprinted with permission. Copyright 2018, Wiley-VCH.

due to its hierarchical structure and high metal content of 67.33%. The H_2 production rate is 2.23 mg h^{-1} at 1.8 V.[66]

3.2. Oxygen evolution reaction (OER)

As a crucial half-reaction in the process of water splitting, the OER is the bottleneck in the electrochemical water splitting because of its multi-electron transfer and sluggish reaction kinetics.[67,68] Compared to two-electron transfer of HER, OER follows a four-electron proton reaction which requires more energy (a higher overpotential) to overcome the kinetic energy barrier.[69,70] Therefore, the development of high efficiency and low cost OER electrocatalysts is important to drive water splitting.[71] Traditional highly active OER electrocatalysts such as carbon-supported noble metals and RuO_2 or IrO_2, are excessively costly and unstable under anodic (charging) conditions.[72] Consequently, the use of waste and naturally abundant sources to produce eco-designed electrocatalysts has attracted tremendous attention. This section highlights the representative OER electrocatalysts from spent batteries, biomass, and other waste materials.

Spent batteries for OER catalysts. Critical valuable metals such as Co, Mn, Ni and Li can be extracted from waste cathodes of spent LIBs.[73] For example, Co from spent LIBs can be converted into $Co(OH)_2$, which then participate in the synthesis of high-temperature (HT) $LiCoO_2$ with the aid of Li_2CO_3.[74] Electrochemical conversion of metal-containing solid wastes can also produce high-performance electrocatalysts.[75] Huang *et al.* exfoliated spent cathode materials of $LiCoO_2$ with strong Li–O interplanar bonding to produce CoOOH nanosheets through a positive bias driven exfoliation strategy. The nanosheets displayed an overpotential of 301 mV at 10 mA cm^{-2} and a Tafel slope of 53.8 mV dec^{-1} (Fig. 5A).[76] The spent $LiCoO_2$ cathode material was also transformed into graded porous Co_9S_8/Co_3O_4 heterojunctions using a combination of conventional hydrometallurgy and calcination sulfidation. The combination of graded porosity and heterostructure promoted OER performance, exhibiting an overpotential of 274 mV at 10 mA cm^{-2} and a Tafel slope of 48.7 mV.[77] In addition, $LiFePO_4$ in spent batteries can also be regenerated into efficient electrocatalysts, successfully achieving the functional transformation from battery electrode materials to electrocatalysts. Cui *et al.* adopted a wetness impregnation method to transfer spent $LiFePO_4$ into a high-performance NiFe oxy/hydroxide OER electrocatalyst. The addition of a nickel promoter and *in situ* transformation substantially increase the electrochemically active area and conductivity as well as synergistically enhance the intrinsic activity, realizing desirable OER performance (overpotential of 285 mV at 10 mA cm^{-2} and Tafel slope of 45 mV dec^{-1} (Fig. 5B).[78] Similarly, $Ni_{0.5}Mn_{0.3}Co_{0.2}O_2$, which is prepared by removing lithium from spent batteries through mechanochemical activation, acts as an efficient OER electrocatalyst.[26] Moreover, Chen and co-workers employed a one-pot boronization procedure that directly transforms spent $LiNiCoMnO_2$ batteries into mixed metal boride (NiCoMnB) materials as effective OER electrocatalysts. The spent batteries underwent a series of standard procedures to produce the brownish leachate, followed by chemical reduction with $NaBH_4$ to yield the final product. The optimized electrocatalyst exhibited outstanding OER performance, and the overpotential can reach up to 372 mV even at a high current density of 500 mA cm^{-2} (Fig. 5C).[79]

Different from the above method of delithiation in spent batteries, Lv *et al.* developed a green recovery method of delithiation driven by a direct current electric field to generate OER electrocatalysts (Fig. 5D). Due to the exfoliation effect, Li^+ are delithiated from the original layered cathode material, resulting in a lamellar structure of delithiated $Li_{1-\delta}Ni_{0.5}Co_{0.2}Mn_{0.3}O_2$ electrode materialswith high specific surface area and large total pore volume, which was verified to display excellent OER performance with an overpotential of

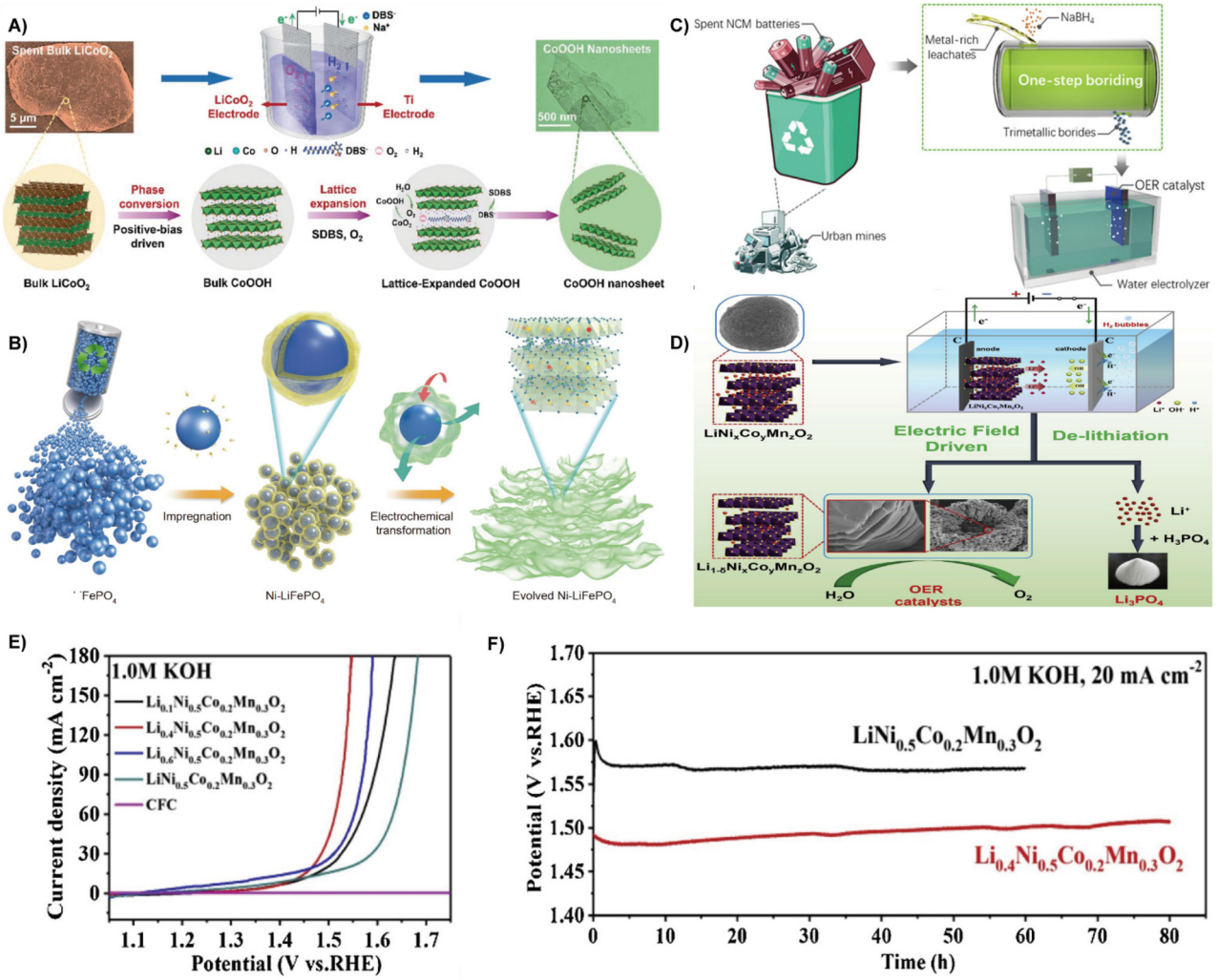

Fig. 5 (A) Schematic illustration of the *in situ* positive-bias driven exfoliation of $LiCoO_2$ into CoOOH.[76] Reprinted with permission. Copyright 2022, The Royal Society of Chemistry. (B) Schematic illustration of the entire regeneration route of spent $LiFePO_4$.[78] Reprinted with permission. Copyright 2021, Springer. (C) Schematic illustration on the synthesis of magnetic NCMB OER electrocatalysts from the spent LIB leachate *via* a facile boriding process.[79] Reprinted with permission. Copyright 2021, The Royal Society of Chemistry. (D) Schematic illustration of the electric field driven de-lithiation process for recycling the ternary $LiNi_xCo_yMn_zO_2$ electrode materials. (E) Polarization curves at 20 mA cm^{-2}. (F) Long-term chronopotentiometric stability of $Li_{0.4}Ni_{0.5}Co_{0.2}Mn_{0.3}O_2$ and $LiNi_{0.5}Co_{0.2}Mn_{0.3}O_2$ at 20 mA cm^{-2}.[80] Reprinted with permission. Copyright 2021, Elsevier.

236 mV at 20 mA cm^{-2} (Fig. 5E), a Tafel slope of 66 mV dec^{-1}, and an exceptional durability of over 80 h (Fig. 5F).[80] Besides, spent zinc-carbon batteries are also valuable sources. Rifat Farzana *et al.* established a sustainable route for the fabrication of manganese oxide (Mn_3O_4) from spent Zn–C batteries under alkaline conditions, which was utilized as a electrocatalyst for the OER.[81]

Biomass for OER electrocatalysts. Biomass is a kind of sustainable and economical material for preparing OER electrocatalyst.[82] Biomass based carbon will substantially increase the electrical conductivity and OER performance.[83] The metal/heteroatom doping tunes the electronic property and offers various metal–carrier interactions which ensure a superior performance.[84,85] Li and co-authors described a straightforward method for converting agricultural cornstalks into bifunctional ORR/OER electrocatalysts doped with Co, Fe, B, and N through hydrothermal reactions and carbonization procedures. The abundant hydrophilic groups (*e.g.*, hydroxyl groups) in the native corn stalks' hierarchically porous structures allows them to combine transition metals (*e.g.*, Co, Fe, Zn) and heteroatoms (*e.g.*, B, N) in a hydrothermal reaction. The pyrolysis and evaporation of Zn^{2+} under high temperature carbonization promoted the formation of a porous structure, thus increasing the specific surface area by 941.44 m^2 g^{-1} and preventing the aggregation of adjacent transition metals. In addition, the synergistic effect of N, B, Fe and Co doping in layered porous carbon further improves the activity and stability of the OER electrocatalyst (Fig. 6A). The material carbonized at 800 °C showed a lowest overpotential of 383 mV at a current density of 10 mA cm^{-2} and a Tafel slope of 100.92 mV

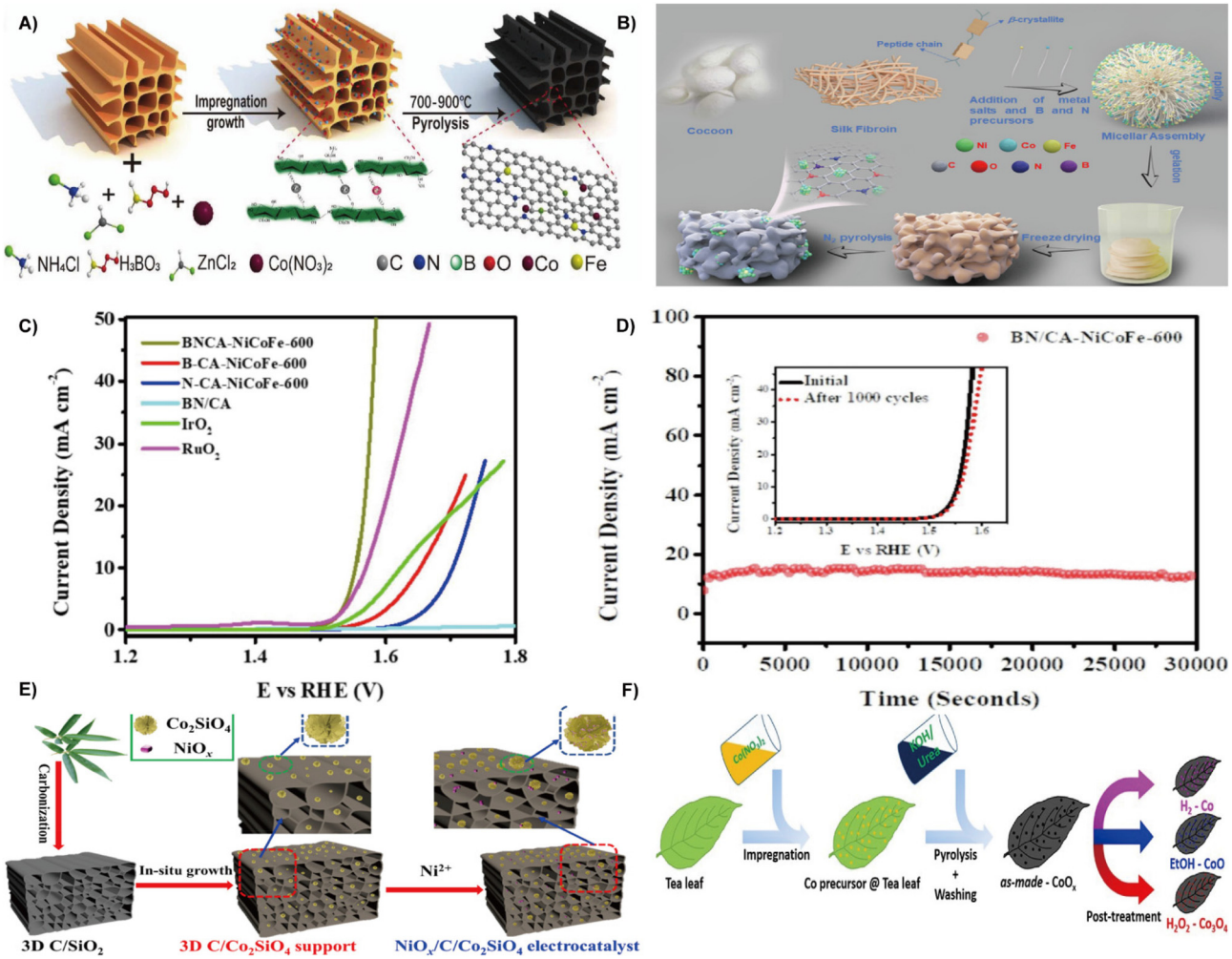

Fig. 6 (A) Schematic illustration of the synthesis methods for ORR/OER catalysts.[86] Reprinted with permission. Copyright 2022, Wiley-VCH. (B) Schematic illustration of the BN/CA-NiCoFe fabrication process. (C) OER polarization curves of electrocatalysts at a scan rate of 5 mV s^{-1}. (D) Chronopotentiometric response of BN/CA-NiCoFe-600 at an uninterrupted current density of 10 mA cm^{-2} for 30 000 s (inset: LSV curves for BN/CA-NiCoFe-600 recorded before and after 1000 cycles).[87] Reprinted with permission. Copyright 2022, Elsevier. (E) Schematic illustration of the synthesis of the $NiO_x/C/Co_2SiO_4$ electrocatalyst.[90] Reprinted with permission. Copyright 2022, Elsevier. (F) Illustration of the synthesis procedure for Co-based nanoparticles supported on activated carbon using tea leaves as a carbon source and templates, and the adjustment of the crystal structure of cobalt *via* post-treatment.[91] Reprinted with permission. Copyright 2021, Wiley-VCH.

dec^{-1}.[86] Subsequently, waste corn stalks (CSs) was used as a multifunctional template for the fabrication of nickel/nickel oxide-nitrogen self-doped carbon (Ni/NiO-NC) nanosheets for HER and OER electrocatalysts by the impregnation–calcination technique.[49] Moreover, Lu and co-workers embedded boron and nitrogen into silk for the preparation of carbon aerogels, and then integrated them with nanoscale nickel–cobalt–iron alloy to prepare a nitrogen co-doped/biomass-derived 3D carbon aerogel OER electrocatalyst (Fig. 6B). Due to the increased number of active sites and enhanced electron transport, BN/CA-NiCoFe-600 delivered an overpotential of 321 mV at a current density of 10 mA cm^{-2} (Fig. 6C) and good stability (Fig. 6D).[87]

In addition, electrocatalyst with multi-dimensional structures can increase the number of active sites.[88,89] Pei and co-authors developed a 3D porous carbon/cobalt silicate (C/Co_2SiO_4) from bamboo leaves as a substrate for nickel oxide (NiO_x) species to prepare a $NiO_x/C/Co_2SiO_4$ electrocatalyst. As depicted in Fig. 6E, the bamboo leaves were carbonized to form 3D carriers, which were treated by hydrothermal method in the presence of Co^{2+}, followed by precipitation of NiO_x nanoparticles on the surface of 3D C/Co_2SiO_4 to produce $NiO_x/C/Co_2SiO_4$. The $NiO_x/C/Co_2SiO_4$ has a significant electrochemically active surface area, thus exhibiting a low overpotential of 355 mV at 10 mA cm^{-2} and a small Tafel slope of 40 mV dec^{-1}.[90] By using spent tea leaves (STLs) as template and sustainable carbon source, Alexander Bähr *et al.* created a variety of cobalt-based nanoparticles supported on activated carbon (Fig. 6F). Typically, the material was treated with either H_2O_2, ethanol vapor, or H_2 to selectively adjust the crystal structure

and oxidation state of the cobalt (including Co_3O_4, CoO, and Co). The ethanol vapor treatment produces the most efficient electrocatalyst, exhibiting high stability for 10 h at 10 mA cm^{-2} and the mass activity of Co reaches up to 2.9 A mg^{-1}.[91] The STLs can also be fabricated as trifunctional electrocatalysts *via* a carbothermal reduction strategy, and cobalt nanoparticles are evenly distributed in porous carbon networks.[92]

By using waste grapefruit peels as the carbon source, He *et al.* constructed nitrogen-doped carbon-encapsulated NiFe alloys and nitrogen-doped graphitized carbon substrate (NiFe@NC/NGC) composites *via* the impregnation–pyrolysis strategy at different temperatures and Ni/Fe ratios.[58] Waste onion peels were transformed into core–shell Fe_3C@N-doped carbon as a reliable OER electrocatalyst.[93] In conclusion, natural carbon sources obtained from biomass are economical and eco-friendly materials for creating high-quality composite electrocatalysts.[94] The preparation of efficient OER electrocatalysts from waste biomass is a good choice depending on different synthesis approaches.[95]

Other wastes for OER electrocatalysts. In addition, spent catalysts with rare precious metal, and waste electronics with available precious metals and plastic, can also be fully explored for value added utilization.[96,97] As for spent catalysts, Muhammad Awais Khan *et al.* reused waste methane reforming catalysts to develop bifunctional electrocatalysts by *in situ* deposition of MoS_2 on waste catalysts (Fig. 7A). At 25 mA cm^{-2}, the as obtained MoS_2@CNF and MoS_2@GC achieved excellent OER performance with overpotential of 154 mV (Fig. 7B) and Tafel slopes of 71 mV dec^{-1}, respectively.[98] Meanwhile, MoS_2@CNF and MoS_2@GC clearly indicate good electrochemical stability (Fig. 7C). Under air atmosphere, the impregnated spent methane reforming catalyst (NAlCNTs-750) containing Ni and other transition metals is calcined to regenerate new NAlCNTs-750, which can be used for OER (Fig. 7D). The novel NALCNTs-750 contains multi-walled carbon nanotubes supported on nickel nanoparticles and porous aluminaexhibits excellent electrochemical activity (370 mV overpotential at 10 mA cm^{-2} and a Tafel slope of 119 mV dec^{-1}).[99] Additionally, e-waste contains valuable metals, such as Li, Ag, Au, W, Se, Te, Ni can also be regarded as active species of electrocatalysts.[100]

3.3. Oxygen reduction reaction (ORR)

The ORR is the core of many fuel cells which holds an important role in the fields of electrocatalysis and metal–air batteries.[101–103] The ORR produces an electrical potential when molecular oxygen is electrochemically reduced by four protons and electrons to generate water.[104] However, the sluggish ORR activity and the high price of platinum group metal electrocatalysts greatly limited their large-scaleapplication.[105] Waste derived ORR electrocatalysts are gradually becoming a substitute for traditional precious electrocatalysts.[106] Accordingly, recent studies have provided different approaches to develop economical and green strategies by converting hazardous wastes into valuable ORR electrocatalysts for energy applications.[107] The following are the research advances in recent years to make full use of spent batteries, waste biomass, and waste plastics to synthesize ORR electrocatalysts.

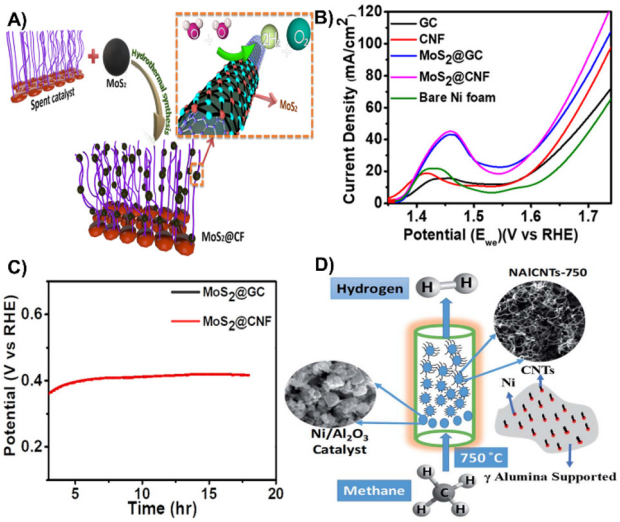

Fig. 7 (A) Schematic illustration for utilizing the spent reforming catalyst for electrochemical water splitting. (B) Linear sweep voltammetry polarization curve for different catalysts. (C) Linear sweep voltammetry results after the stability test.[98] Reprinted with permission. Copyright 2021, American Chemical Society. (D) Schematic diagram for the methane decomposition process and the composition of the spent catalyst (NAlCNTs-750).[99] Reprinted with permission. Copyright 2021, The Royal Society of Chemistry.

Spent batteries for ORR electrocatalysts. Converting spent batteries into ORR electrocatalysts can effectively reduce chemical consumption and secondary pollution. Graphite from cathodes of LIBs can be recycled and used to prepare carbon-based catalysts.[108] Ruan *et al.* synthesized iron–nitrogen-doped carbon-based composites by mixing waste graphite, $Fe_2(SO_4)_3$, and polyaniline, followed by pyrolysis to yield an optimized electrocatalyst, denoted C-PANI-Fe. Using waste graphite as a substrate, the resulting C-PANI-Fe showed a large surface area (517.13 m^2 g^{-1}), a high nitrogen content (61%), and exhibited an onset potential of 0.91 V and a half-wave potential of 0.8 V, suggesting a Pt-like ORR activity (Fig. 8A).[14] Spent graphite in LIBs could act as a precursor to prepare nitrogen-doped graphene (NG-Bat) as a valuable eletrocatalyst for the ORR, exhibiting an onset potential of 0.867 V.[109]

By employing Co and Fe from spent LIBs as metal precursors and sawdust-derived carbon as carbon sources, Jiao *et al.* reported the design of a bifunctional CoFe/C catalyst for efficient OER and ORR. As for the CoFe/C electrocatalyst, due to the electrostatic attraction between Co^{3+} and Fe^{3+} and the hydroxyl groups in the sawdust, the CoFe nanoparticles can be uniformly dispersed on sawdust-based carbon, exhibiting excellent electrocatalytic performance with a long stability of 350 h and a large discharge voltage (1.25 V at 10 mA cm^{-2}) (Fig. 8B).[110] The combination of valuable metal oxides from LIB cathodes (LCO) and anodes (graphite) to prepare a Co_3O_4/rGO composite has been proposed and investigated as an ORR

electrocatalyst, which exhibits good ORR activity with an onset potential of 0.936 V (Fig. 8C) as well as stability (Fig. 8D).[111]

Biomass for ORR electrocatalysts. Biomass with a versatile morphology, abundant heteroatoms, and easily available precursors has become one of the research focuses for ORR.[112] Xie and co-authors presented a scalable approach to prepare Co, N Co-doped carbon (CoNC) materials from organic-rich chitosan waste for ORR, yielded a limiting current of ~5.36 mA cm^{-2} and an onset potential of −0.105 V *vs.* Ag/AgCl.[113] Red dates can be used as a carbon source and g-C_3N_4 as a sacrificial template and nitrogen source to fabricate a 3D porous structure (Fe–N–C) with a nitrogen content of 14.83%, the as resulted ORR electrocatalyst exhibited a half-wave potential of −0.05 V.[114] Different from the above monometallic electrocatalysts, the mixed metal electrocatalysts have better performance because of their optimized electronic structure and more active sites. By using tobacco stems as the carbon precursors and the incorporation of the NiCo alloy and N heteroatom, an ORR and OER bifunctional electrocatalyst was prepared under a two-step pyrolysis process. The incorporation eventually alters the electronic structure, produces abundant active sites and results in excellent performance competing Pt/C (a starting potential of 0.92 V and a half-wave potential of 0.86 V) (Fig. 9A).[115] Moreover, Ahsan *et al.* reported a carbothermal reduction method for the synthesis of cobalt-doped porous carbon (Co@PC) electrocatalysts by directly carbonizing a mixture of waste tea and cobalt nitrate. By regulating the gathering process of electrons at the defective carbon interface, the electronic and surface properties of Co@PC can be effectively adjusted, thereby promoting electron transfer and boosting the ORR activity. Therefore, Co@PC-7 (700 °C) exhibits a good ORR performance with an onset potential of 0.946 V and a half-wave potential of 0.86 V (Fig. 9B).[92]

Waste plastic for ORR electrocatalysts. Most plastics are derived from synthetic polymers, which are difficult to degrade, causing serious environmental concerns.[116] Developing advanced materials from plastic waste through a variety of synthetic strategies is an attractive way from an environmental and financial standpoint.[117] For instance, by using a two-stage pyrolysis and chemical vapor deposition technique from polyethylene (PE), Andrei Veksha *et al.* created a new nanocomposite ($CaCr_2O_4$/CNPs) made of α-$CaCr_2O_4$ spinel plates connected with carbon nanoplatelets (CNPs) from mixed polymers yields an overpotential of 0.27 V *vs.* Ag/Ag/KCl at 0.06 mA cm^{-2} (Fig. 9C).[118] Under a similar strategy, pyrolysis of waste plastics with FeNi-based catalysts yields carbon-based bimetallic electrocatalysts (FeNi-OCNTs). Fe–Ni alloy nanoparticles with a unique structure are wrapped in FeNi-OCNTs, which enables the catalyst with exceptional ORR performance, showing a half-wave potential of 0.87 V and an onset potential of 1.01 V (Fig. 9D).[119] Inspired by the above investigations, an extra highly active single atomic site iron–nitrogen–carbon (Fe–N–C) electrocatalyst was formed by combining polyurethane (PU) and polyethylene (PE) with the addition of $FeCl_3$ at a high pH value. The Fe–N–C electrocatalyst exhibited high catalytic activity with a half wave potential range of 0.705–0.722 V.[120] Obviously, the use of plastic waste as a carbon skeleton to obtain an ORR electrocatalyst is an environmentally and economically beneficial approach.[121]

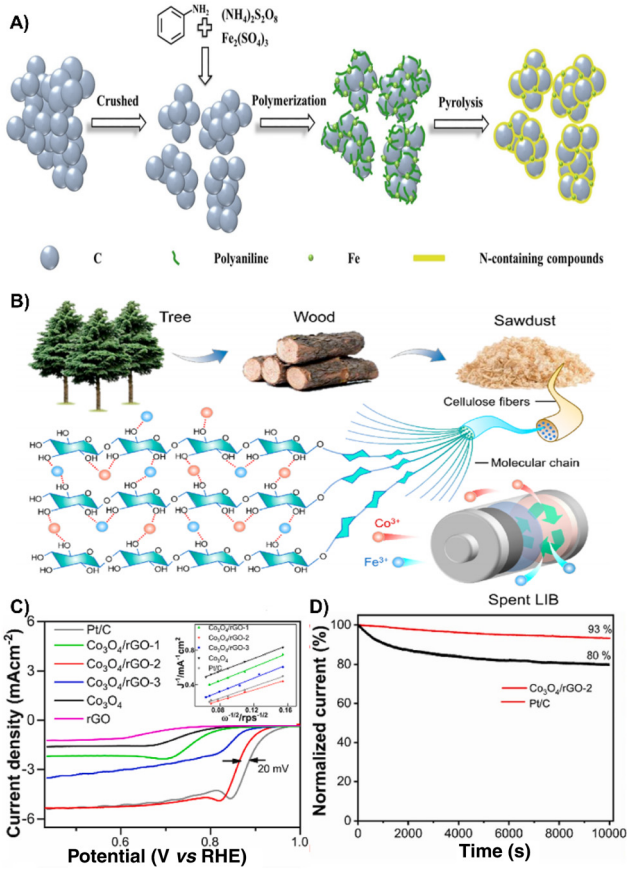

Fig. 8 (A) Schematic illustration of the synthetic process of catalysts.[14] Reprinted with permission. Copyright 2021, Wiley-VCH. (B) Design of the CoFe/C catalyst.[110] Reprinted with permission. Copyright 2022, American Chemical Society. (C) ORR polarization curves of all synthesized samples with Pt/C as a benchmark in O_2-saturated 1 M KOH solution at 20 mV s^{-1} at 1600 rpm electrode rotation (inset, Koutecky–Levich [K–L] plots at 0.636 V *vs.* RHE). (D) Chronoamperometric response of the Co_3O_4/rGO-2 and Pt/C (30%) catalysts at a constant potential of 0.836 V *vs.* RHE.[111] Reprinted with permission. Copyright 2023, Elsevier.

3.4. CO_2 reduction reaction (CO_2RR)

Carbon dioxide (CO_2) contributes to global warming and causes environmental problems.[122] Electrochemical reduction of CO_2 to available fuels is considered as an effective means to reduce carbon dioxide emissions due to its high efficiency, controllable selectivity, easy operation and potential application in industrial chemistry.[123] However, the exploitation of cost effective, highly active electrocatalysts for converting CO_2 to high-value-added hydrocarbon energy sources remains challenging.[124,125] This section outlines the use of waste materials as CO_2 reduction catalysts.

Industrial waste for CO_2RR electrocatalysts. Recycling metals from industrial waste as electrocatalysts for CO_2RR is of great

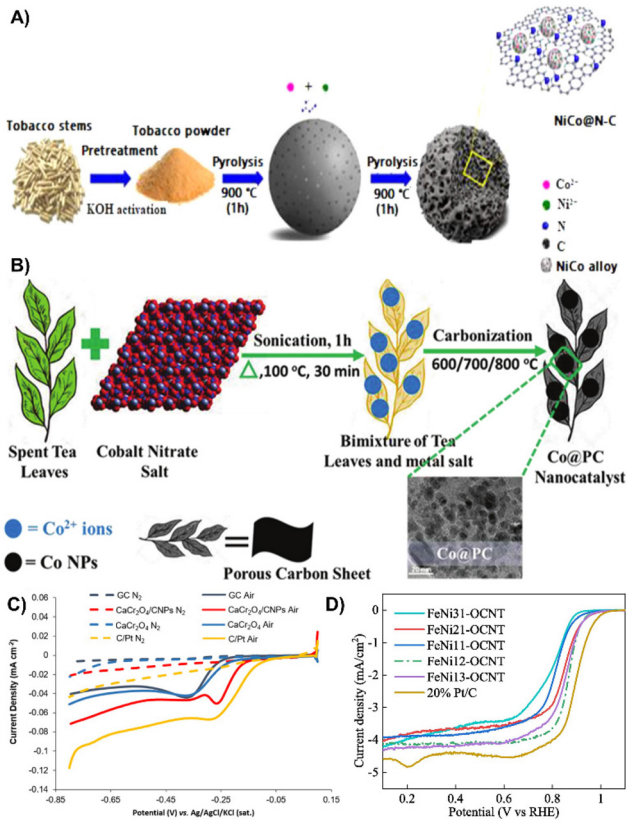

Fig. 9 (A) Schematic illustration of the synthesis of NiCo@N–C.[115] Reprinted with permission. Copyright 2022, Elsevier. (B) Schematic representation of the Co@PC electrocatalyst synthesis process.[92] Reprinted with permission. Copyright 2020, American Chemical Society. (C) ORR of the respective different surfaces in air or N_2 saturated 0.1 M KOH.[118] Reprinted with permission. Copyright 2019, Elsevier. (D) LSV curves of FeNi-OCNTs and of 20% Pt/C in O_2-saturated solutions at 5 mV s^{-1} scan rate and 1600 rpm rotation speed.[119] Reprinted with permission. Copyright 2020, Elsevier.

significance for environmental protection and resource recycling. Copper (Cu) exhibits moderate binding energy towards key reaction intermediates during the electroreduction of CO_2, which enables the production of simple reduction products (C_1 products) and complex reduction products (C_2 products).[126] Therefore, it is an important research direction to transform the copper-containing waste into a valuable electrocatalyst. By using industrial metallurgical wastes as raw materials, Yang *et al.* extracted Cu and lead (Pb) from industrial wastewater by electrodeposition, preparing a series of copper-lead (Cu_xPb_y) materials as CO_2RR catalysts.[33] It is found that there is a synergistic effect between Cu and Pb in the prepared bimetallic electrocatalysts, especially, the Cu^+ and Pb^{2+} species that can be reduced to Cu^0 and Pb^0 metal. The reduced species play an important role in the formation of CO, which promotes the enhancement of CO selectivity (the amount of CO formed at −1.05 V *vs.* RHE is about 4 times that of pure Cu). In addition, Firschke *et al.* used waste industrial Cu–Sn alloy as a raw material through a simple electrochemical method to obtain mesoporous foam as a CO_2RR catalyst (Fig. 10A).[127] The special nanostructure of the Cu–Sn foam surface makes the material exhibit high selectivity for CO (the faradaic efficiency of CO is >85% at −0.8 V *vs.* RHE potential) and great inhibition of the HER (the faradaic efficiency of H_2 is about 5%) (Fig. 10B).

Recycling electronic waste that contains large amounts of metals to prepare a variety of metal catalysts has great economic benefits. As shown in Fig. 10C, Sharma *et al.* successfully recovered several metals from printed circuit boards (PCBs) by low-temperature grinding and dissolution filtration to prepare a CO_2RR catalyst containing multiple metals by one-step ball milling. Studies showed that a variety of metal in the electrocatalyst (large amounts of Cu, Sn, Fe, Al and Ag, and trace amounts of Pb, Sb, Pd and Cr) enabled the formation of bimetallic coordination intermediates, which made the catalyst selectively generate CO and CH_4 in alkaline and neutral media with the CO faradaic efficiency of 84.64%, and the faradaic efficiency of CH_4 is 6.29% at −1.2 V *vs.* Ag/AgCl in a 0.5 M $NaHCO_3$ electrolyte.[128] Although the synthesis of CO_2RR electrocatalysts from waste materials yielded a lower faradaic efficiency of CO than Ni–N–C (85%)[129] and monoatomic iridium (95.6%).[130] The recycling of waste metals as CO_2RR electrocatalysts has great potential for environmental protection and resource recycling.

Biomass for CO_2RR electrocatalysts. Biomass has broad prospects in the field of electrocatalysts because of its low cost, rich abundance, diverse structure, multi-porosity and tunable surface chemical properties.[122] Yao *et al.* used cattail as a raw material to synthesize nitrogen-doped nanoporous carbon sheets by calcination under NH_3 gas flow for the CO_2RR.[131] After KOH activation and calcination at 900 °C, it was found that the carbon sheets had a high surface area, multiple pores and a high pyridine N content, which greatly improved the activity and selectivity, yielded a high CO selectivity at a low overpotential (−0.39 V *vs.* REH, faradaic efficiency of 90%) (Fig. 11A). Inspired by the tunable surface property of biomass, Wang *et al.* reported a highly dispersed Ni–N site embedded in nitrogen-doped porous carbon materials as a CO_2RR electrocatalyst by using tobacco stem as raw a material, N was introduced by N_2 airflow calcination, and Ni was introduced by calcination after soaking in nickel(II) acetate tetrahydrate (Fig. 11B).[132] It was found that the free energy of the key intermediate (*COOH) formed on the highly dispersed Ni–N sites is greatly reduced, and therefore displays a faradaic efficiency of 44.67% (CO) and a current density of 30.96 mA cm^{-2} at an overpotential of 98 mV. Similarly, as depicted in Fig. 11C, Costa *et al.* synthesized a silver–carbon hybrid (Ag@C) as a CO_2RR electrocatalyst by high-temperature carbonization of babassu coconut (BM), which was then pulverized and mixed with silver nitrate solution.[133] After hydrothermal carbonization, the silver nanoparticles are attached to the surface of biomass based carbon nanospheres. As a result, the biomass derived functionalized carbon sphere acts as a CO_2RR electrocatalyst to generate oxalic acid with a faradaic efficiency of 28.95%.

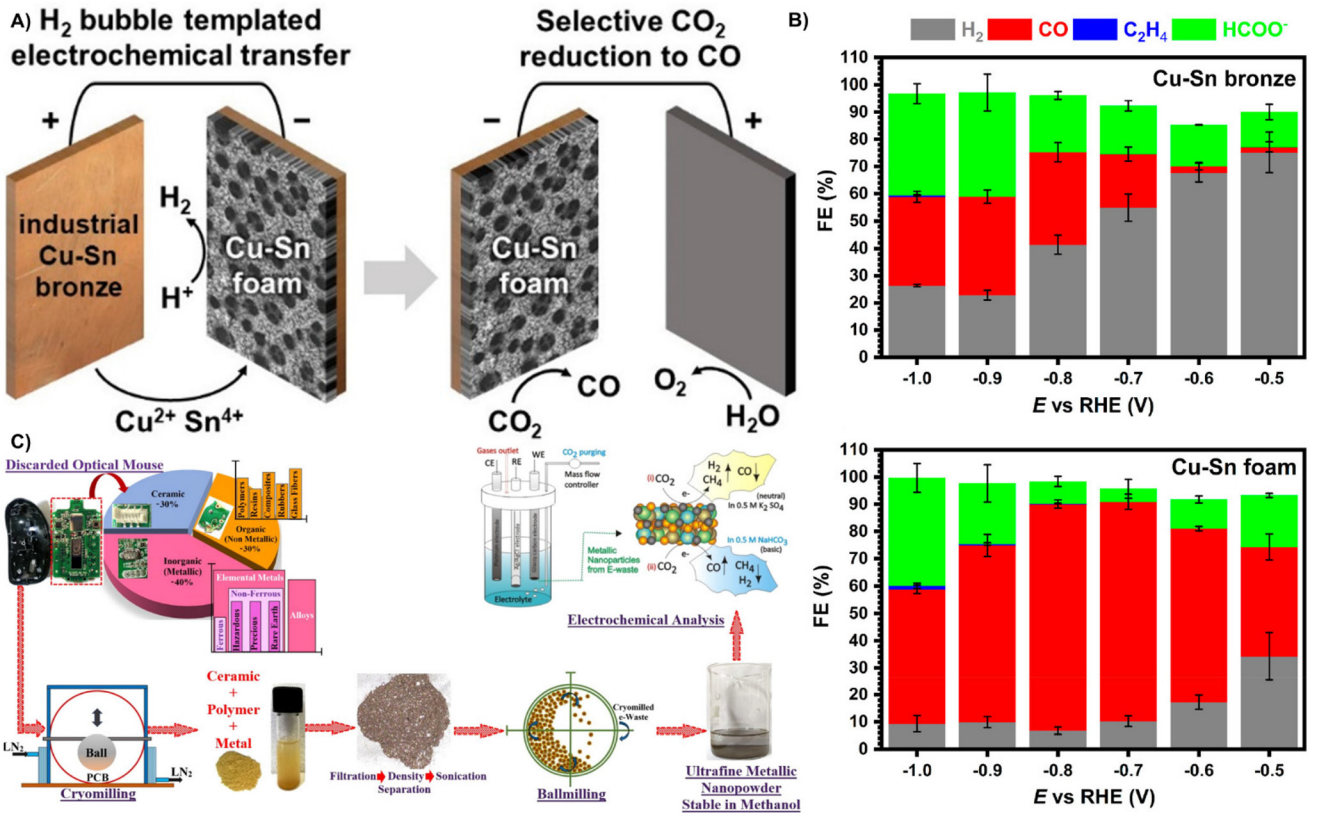

Fig. 10 (A) Mesoporous $Cu_{10}Sn$ foams were obtained by anodic dissolution and cathodic redeposition of $Cu_{14}Sn$ waste bronze under dynamic hydrogen bubble template conditions. The bimetallic foam electrode exhibited high CO_2 electroreduction selectivity. (B) Faradaic efficiency on pristine copper-tin bronze and on copper-tin foam.[127] Reprinted with permission. Copyright 2021, American Chemical Society. (C) Recycling of metal residues from PCB e-waste through a large number of low temperature ball milling and ball milling processes for electrochemical CO_2 selective reduction to CO, CH_4 and H_2.[128] Reprinted with permission. Copyright 2020, American Chemical Society.

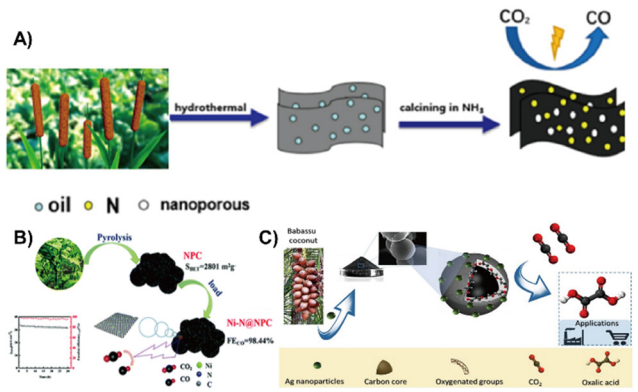

Fig. 11 (A) Nitrogen-doped nanoporous carbon plate made of renewable biomass cattail as a CO_2 reduction catalyst.[131] Reprinted with permission. Copyright 2019, American Chemical Society. (B) Tobacco stem-derived nitrogen-containing porous carbon with highly dispersed Ni–N sites as an efficient electrocatalyst for CO_2 reduction to CO.[132] Reprinted with permission. Copyright 2021, The Royal Society of Chemistry. (C) A novel carbon-silver hybrid material from Baba Su coconut biomass carbon material coupled with silver was prepared electrochemically reduced CO_2 to produce oxalic acid.[133] Reprinted with permission. Copyright 2020, Elsevier.

Waste sludge for CO_2RR electrocatalysts. Metal free electrocatalysts with low cost and high stability have been favored. Moreover, the high electronegativity of nitrogen can effectively change the electronic structure of the carbon skeleton, resulting in polarized active sites. Therefore, nitrogen-doped metal-free carbon is a promising carbon-catalyzed CO_2 electrocatalyst.[134] Municipal sludge, which is rich in heteroatoms such as N and P, is an excellent raw material for the preparation of metal-free carbon. Deng *et al.* presented a carbonization and pyrolysis method to transform municipal sewage sludge directly into nitrogen-doped hierarchical carbon materials, which was used as a CO_2RR electrocatalyst.[28] Further studies showed that the total faradaic efficiency of the three main organic reduction products (C_2H_5OH, CH_3OH and CH_4) reached up to 90.14% and the faradaic efficiency did not decrease significantly during six consecutive cycles. It is noteworthy that carbon dots and doped pyridine-N and pyrrole-N play a vital role in the efficient production of C_2H_5OH (Fig. 12A). In addition, to increase the nitrogen-doped active sites, as shown in Fig. 12B, Qin *et al.* prepared a nitrogen-doped porous carbon (NPC-600) as a CO_2RR electrocatalyst by a hydrothermal process, followed by acid leaching using digested sludge as a raw material and SBA-15 mesoporous

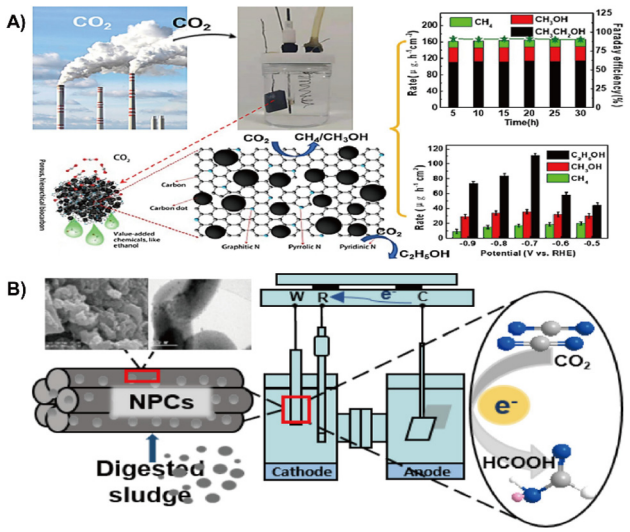

Fig. 12 (A) Municipal sludge derived carbon dots modified, N-doped biochar for the electrochemical reduction of carbon dioxide.[28] Reprinted with permission. Copyright 2022, Elsevier. (B) Nitrogen-doped porous carbon from digested sludge for the electrochemical reduction of carbon dioxide to formate.[135] Reprinted with permission. Copyright 2018, American Chemical Society.

molecular sieve as a template.[135] It was found that the rich pore structure and rough surface structure can expose more nitrogen defect active sites. When used for the CO_2RR in CO_2-saturated $NaHCO_3$, NPC-600 shows a maximum faradaic efficiency of formic acid reaching 68% which was lower than those of Au, Ru, and Ir catalysts (the Ir catalyst for formate generation was 96%),[136] however, the low prices of NPCs (the cost per gram of NPC-600 was 0.74 $) make it stand out from the other electrocatalysts.

3.5. Nitrogen reduction reaction (NRR)

The nitrogen reduction reaction (NRR) is an important ammonia (NH_3) synthesis process in industrial production.[137] The electrochemical NRR has been recognized as a green and sustainable alternative to traditional synthetic processes for NH_3 synthesis.[138,139] Current electrocatalysts focus on selective NH_3 production and high faradaic efficiency due to the high stability of N_2 and HER competition.[140] Recycling waste as NRR electrocatalysts is of great significance in environmental protection and energy conservation.[141] This section discusses the use of waste sludge as an electrocatalyst for the NRR considering the effective strategy, morphology, and NRR performance.

Conversion of sludge and municipal sludge containing a large number of active materials is a feasible way to prepare NRR electrocatalysts. Deng *et al.* used municipal sludge as a raw material to prepare multiple heteroatom co-doped porous carbon for the NRR by calcination and pickling under N_2 atmosphere.[142] The sludge contains a large number of heteroatoms (O, N, P, S), and pickling endows the material with more pores, thus resulted in high activity for NRR with an NH_3 yield of 35.76 μg h^{-1} mg^{-1} cat in 0.1 mol L^{-1} HCl solution at −0.7 V (*vs.* RHE), and a faradaic efficiency of 7.79% (Fig. 13A). Zhang *et al.* prepared two types of electroplating sludge precipitated from chromium and copper electroplating wastewater by washing, ball milling and calcination, followed by alkali treatment to obtain a $CuCr_2O_4$ octahedral spinel-like NRR electrocatalyst.[143] They found out that the electrocatalyst has a high specific surface area (18.9 m^2 g^{-1}) and abundant oxygen vacancies, resulting in higher NRR catalytic activity with an NH_3 yield of 15.9 μg h^{-1} mg^{-1} cat, which is comparable to those of conventional catalysts (Fe_2O_3: 15.9 μg h^{-1} mg^{-1} cat; TiO_2: 15.1 μg h^{-1} mg^{-1} cat) (Fig. 13B), and the faradaic efficiency reaches a maximum of 0.9% at −0.83 V.

Directly converting waste into NRR electrocatalysts in the NRR meets the requirement of sustainable development of clean energy. However, the lithium-mediated method relies on the formation of lithium nitride at the cathode of an electrochemical cell, and this intermediate reacts with a proton source to produce ammonia, which is recognized as the most promising reaction for improving the ammonia yield and has a promising application in waste utilization.[144,145]

In general, in the field of electrocatalysis, biomass, spent batteries, waste plastics, sludge and waste e-waste can be converted into electrocatalysts by calcination, hydrothermal and wet chemical methods. Biomass and waste plastics can be converted into porous carbon, but the pyrolysis process generates large amounts of tar and organic molecular gases, which destroy the pore channels of the carbon material and require additional purification, thereby complexifying the procedure. While for electrocatalysts, metal active sites are necessary to improve the activity and selectivity. Spent batteries rich in Ni, Co, Mn, and Fe active metals can be used in electrocatalysis alone or as complexes. The lack of a unified synthetic route for recycling spent LIBs increases the difficulty of recycling. Sludge contains a large amount of metallic and non-metallic elements, which can be extracted as active sites for electrocatalysts or pyrolyzed into heteroatom-doped carbon materials. However, the composition of sludge is complex and contains a large amount of organic matter, heavy metals, pathogens, *etc.* Their reuse requires adequate treatment and safety measures. The recycling of waste materials in electrocatalysis is promising, and the various metals and carbon materials contained in the waste materials are necessary to improve the electrocatalytic activity and selectivity, but the purification and treatment of pollutants needs to be solved.

4. Waste to wealth in energy storage

As an attractive energy storage technology, LIBs, LSBs, LOBs, SIBs, KIBs, ZIBs, ZABs, and supercapacitors are experiencing unprecedented rapid development.[146,147] Waste containing active metals and carbonaceous materials provides an energy conservative and eco-friendly way for the preparation of elec-

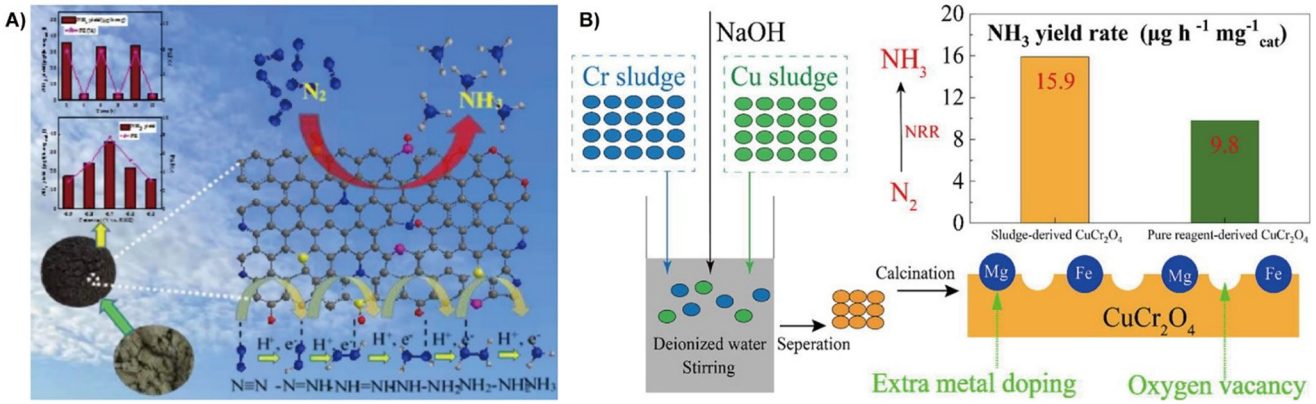

Fig. 13 (A) Municipal sludge-derived porous carbon co-doped with multiple heteroatoms effectively electrocatalytically reduces N_2 to ammonia under certain environmental conditions.[142] Reprinted with permission. Copyright 2022, Elsevier. (B) Chromium and copper plating wastewater is synthesized into electrocatalysts by three different methods, including water washing, ball milling and alkali treatment before calcination.[143] Reprinted with permission. Copyright 2022, Elsevier.

trode materials for energy storage. For example, Li, Co, Ni and Mn serve as active species to form cathode materials with high electrical conductivity and stability in secondary batteries.[148] Si-containing waste can be converted into Si nanomaterials to replace conventional graphite anodes. Biomass and plastic derived porous carbon with a large specific surface area act as anode materials or surface coatings of cathode. Depending on the type, composition, structure, and morphology of the waste, diverse applications from waste have been developed.[9,34] This part reviews the progress of versatile types of waste materials in the field of LIBs, LSBs, LOBs, SIBs, KIBs, ZIBs, ZABs and supercapacitors.

4.1. Lithium-ion batteries (LIBs)

Spent batteries for LIBs. Capacity degradation is inevitable in the life of LIBs, in which the deterioration of cathode performance arises from the deactivation of active materials.[149] While the deactivation of the anode is mainly due to the partial dissolution of an active substance or electrolyte solvent oxidation during the cycling/storage process, resulting in capacity decline.[150] Spent LIBs containing various kinds of transition metals (such as Li, Ni, Co, and Mn) and graphite can be effectively regenerated for energy storage, which can solve the problem of metal scarcity and environmental pollution.[151,152] For example, spent LIBs were dissolved in oxalic acid in which the transition metal was precipitated and deposited on the waste $Li(Ni_{1/3}Co_{1/3}Mn_{1/3})O_2$ (NCM) cathode surface. The addition of a small amount of Li_2CO_3 to unreacted NCM under calcination can directly fabricate new submicrometer-sized NCM cathodes while maintains the optimal element ratio (Fig. 14A). The regenerated NCM electrode delivers an initial specific discharge capacity of 168 mA h g^{-1} at 0.2 C and an excellent capacity retention of 91.5% after 150 cycles (Fig. 14B).[153]

The spent $LiFeO_4$ was treated by microwave and chemical lithiation to produce new $LiFeO_4$. It is noted that the newly produced $LiFeO_4$ shows the same olivine structure as the original one with a preserved carbon layer, enabling the regenerated electrode with a comparable performance compared to the fresh one. When applied to LIBs, it produces a reversible capacity of 145 mA h g^{-1} at 1 C and even reaches up to 107 mA h g^{-1} at 10 C, while the capacity retention is kept at 96% at 5 C after 300 cycles.[154] Moreover, a simple and economic way is to treat the waste $LiNi_{0.6}Co_{0.2}Mn_{0.2}O_2$ cathode through ammonia leaching, co-precipitation combined with a solid phase reaction to produce regenerated $LiNi_{0.6}Co_{0.2}Mn_{0.2}O_2$. The recycled cathode displays an initial discharge capacity of 178.4 mA h g^{-1} at 0.1 C and a capacity retention of 92.1% at 0.5 C after 100 cycles.[155] Through a closed cycle system, lithium species can be recycled from lithium graphite and converted into Li_2CO_3 after absorbing CO_2, which was used for the direct regeneration of $LiCoO_2$ and $LiNi_{0.5}Mn_{0.3}Co_{0.2}O_2$. The regenerated $LiCoO_2$ delivers a capacity of 130 mA h g^{-1}, while the degraded graphite yields a capacity of 370 mA h g^{-1}, comparable to those of commercial LIBs.[15]

Graphite serves as a commercial anode in LIBs with long cycling stability and high electrical conductivity.[18] Xiao *et al.* found that waste LIB anodes enable the volatilization of the binder and electrolyte in the spent graphite rapidly under the microwave field, which can simply realize the separation of spent graphite (Fig. 14C). Moreover, microwave radiation converted the lithium remaining in the waste graphite to Li_2CO_3 in the subsequent process. After water immersion and heating, the regenerated graphite (RG) shows high purity and ordered layered structures, thereby delivering an initial discharge capacity of 435.2 mA h g^{-1} at 0.1 C and a Coulomb efficiency of 80.6%. In addition, the regenerated graphite showed excellent cycling performance at 0.5 C, and the capacity retention rate was 96.6% after 100 cycles, comparable to that of commercial graphite (CG) (97.1%) (Fig. 14D).[156] Using spent graphite as the core and asphalt as the coating carbon source, Xiao *et al.* prepared asphalt carbon@graphite composites by impregnation and pyrolysis treatment (Fig. 14E). High temperature treatment and asphalt coating not only improve the

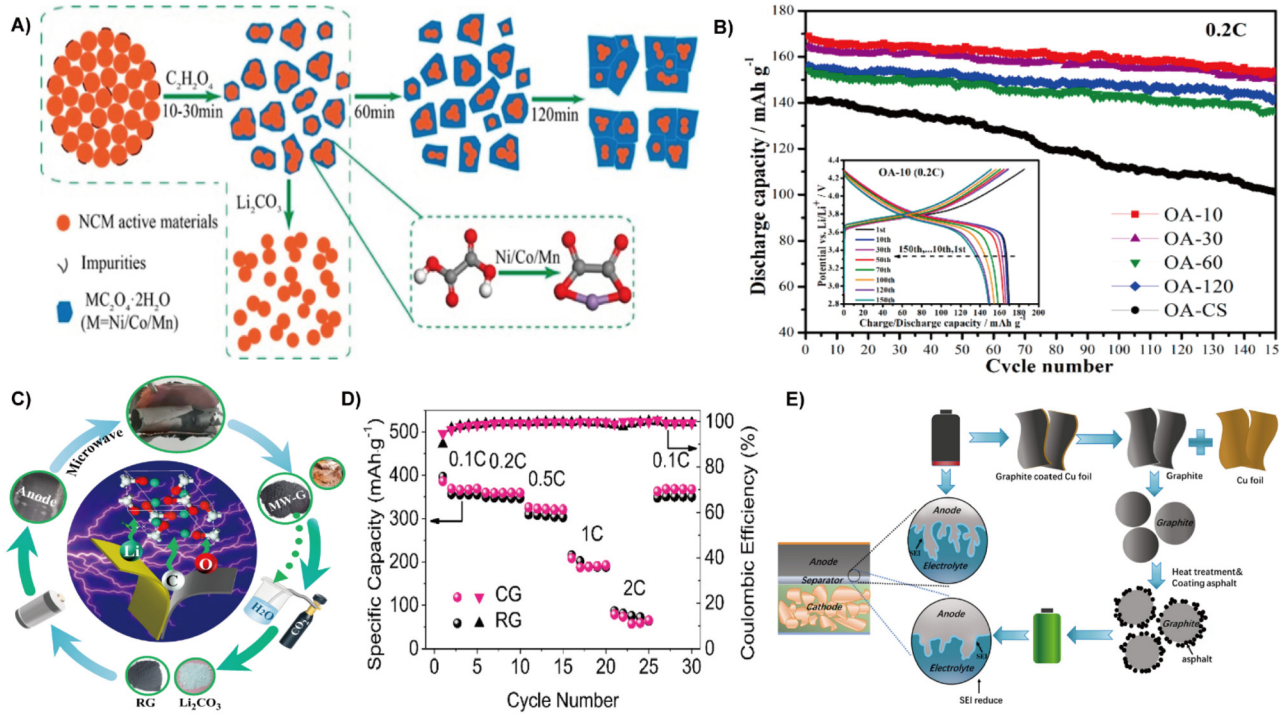

Fig. 14 (A) Illustration of the regeneration process of spent NCM materials with oxalic acid leaching and calcination. (B) Cycling performances at 0.2C (inset shows the charge/discharge curves of OA-10 at different cycles).[153] Reprinted with permission. Copyright 2018, American Chemical Society. (C) Flowchart of recycling of the spent LIB anode. (D) Rate capabilities of RG and CG electrodes at different current densities.[156] Reprinted with permission. Copyright 2022, Elsevier. (E) Schematic diagram of coating asphalt on the spent graphite anode.[157] Reprinted with permission. Copyright 2022, Springer.

degree of graphitization, but also shape a smooth surface morphology of spent graphite. Therefore, the as prepared material leads to a high specific capacity of up to 403 mA h g^{-1} at 0.1 C along with a capacity retention of 97.8% at 0.1 C over 110 cycles, comparable to those of fresh graphite electrodes.[157]

Besides, spent graphite can be combined with silicon to produce carbon coated silicon treated T-SGT/Si@C which can effectively reduce the volume expansion to form a porous structure when used as an anode. The as-prepared anode displays a capacity of 434.1 mA h g^{-1} at 500 mA g^{-1} and a capacity retention of 92.47% after 300 cycles.[158] Recycling waste carbon residue (WCR) from waste LIBs also has an important impact on both economic and environmental benefits.[159] Using stannous chloride ($SnCl_2$) as the reducing agent, Zhu *et al.* prepared high-performance nano-Sn/G@C composite anodes with a sandwich structure by carbothermic reduction, taking advantage of the defect characteristics of the WCR surface with severe oxidation and porous structure. Because nano-Sn has an atomically dispersed structure, it is important to maintain the structural integrity. As a result, the material exhibits good cycling performance as an anode with a reversible capacity of 607.6 mA h g^{-1} after 500 cycles.[160]

Silicon waste for LIBs. Owing to its outstanding specific capacity and rich abundance, silicon has become a substitute material for graphite anodes, and has been extensively studied in LIBs.[161] However, their practical application is hampered by substantial volume expansion and deterioration of the electrode structure during cycling with suppressed electrochemical performance.[162] Industrial waste contains a large amount of silicon that can be recycled for high value-added materials.[163] Waste glass microfiber filters (GFs) can be used as the best silica resource for nanostructured silicon synthesis. Using GF as a silicon precursor and a carbon coated hard template, Kang *et al.* prepared a silicon/carbon composite suspension electrode with a fibrous yolk–shell structure using magnesium thermal reduction and carbon coating processes (Fig. 15A). The conductive carbon shell acted as a framework and confined the silicon nanoparticles to form a yolk–shell structure to control the volume expansion of silicon nanoparticles (Si NPs), showing a high capacity of 2.2 mA h cm^{-2} after 150 cycles.[164] Similarly, by utilizing waste micron-scale silicon wafers as precursors and adding sucrose carbon coating materials, low-cost carbon-coated SiNPs (Si@C) can be easily produced by high-energy mechanical milling (HEMM). The nanostructure and voids of the carbon-coated SiNPs enhanced the electrochemical performance, providing a high specific capacity of 948 mA h g^{-1} at 0.5 C and after 500 cycles when used as an anode.[165]

The waste photovoltaic material with silicon is also an ideal material for silicon anode preparation.[163] Xian *et al.* used an improved silver-assisted chemical etching process to treat the raw photovoltaic silicon cutting waste to prepare a porous

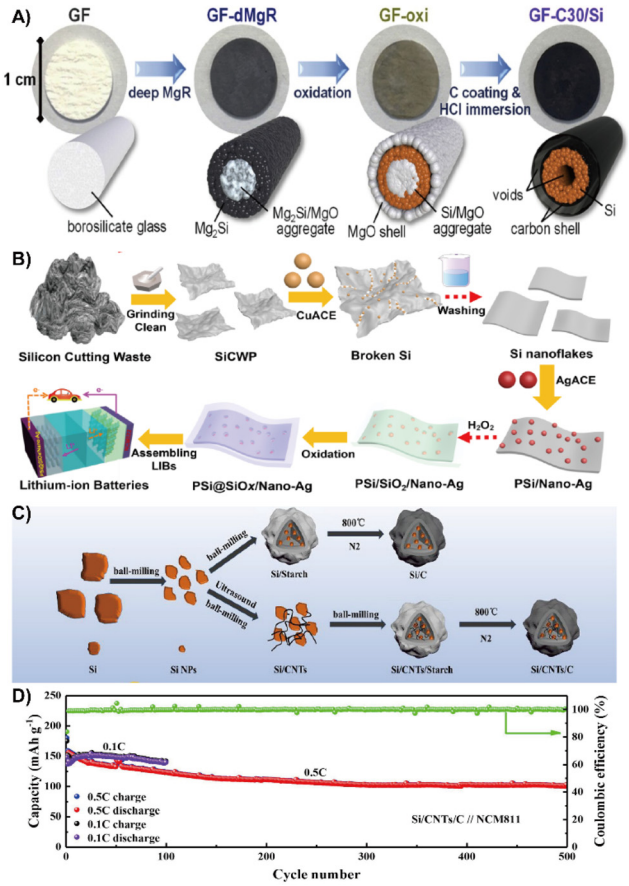

Fig. 15 (A) Preparation process diagram of the GF-C30/Si suspended electrode.[164] Reprinted with permission. Copyright 2020, Elsevier. (B) Fabrication of the Si@SiO_x/Nano-Ag composite.[32] Reprinted with permission. Copyright 2021, Elsevier. (C) An overall illustration of a typical recovery and conversion process. (D) Long-term cycling performance at 0.5 C.[167] Reprinted with permission. Copyright 2022, Elsevier.

Si@SiO_x nanosilver composite with nano/micropores and a natural SiO_x layered structure (Fig. 15B). The lamellar structure of nano/micropores and the natural SiO_x layer solves the volume expansion of Si, while the incorporation of Ag nanoparticles greatly improves the conductivity of the composites and promotes the electron transfer. The reversible capacity after 500 cycles reaches up to 1409 mA h g^{-1}.[32] To effectively reduce the limitations of deep oxidation and trace impurity entrainment in the recovery of photovoltaic waste silicon, Lu *et al.* proposed an electrothermal shock method that can directly convert photovoltaic waste silicon into silicon nanowire (SiNW) electrodes. The SiNWs have an ultra-high area loading of 4.02 mg cm^{-2}. When used as an adhesive-free anode for LIBs, it shows a large areal capacity of 3.2 mA h cm^{-2} after 600 cycles.[166] Wang *et al.* mixed the nano-silicon obtained from grinding waste silicon powder with carbon nanotubes and PVP to prepare core–shell Si/CNTs/C composites by wet ball milling and high temperature pyrolysis (Fig. 15C). The core–shell structure effectively alleviates the volume variation of silicon, ensuring good long-term stability and high-capacity retention performance with a capacitance loss of 0.064% after 500 cycles at 0.5 C (Fig. 15D).[167]

Biomass for LIBs. Biomass and its derived composites benefit from low cost, green synthesis and simple accessibility, which are widely studied to serve the sustainable development strategy.[23] Intensive research studies have been reported to investigate the feasibility of converting renewable biomass to electrode materials.[168] Waste biomass with a high carbon content, such as Eichhornia crassipes, can be used as an alternative to conventional graphite anodes to further increase the battery capacity. Chen *et al.* converted the floating waste Eichhornia crassipes into honeycomb biochar as the negative electrode of LIBs through KOH activation during carbonization. Among them, the cellular porous structure promotes the transfer of Li^+ and the penetration of electrolytes, displaying an excellent capacity of 229.7 ± 0.9 mA h g^{-1} at 3000 mA h g^{-1} (Fig. 16A), and a capacity retention of 720 ± 30.2 mA h g^{-1} after 200 cycles.[21]

Combining biomass-based carbon with other nanocomposites, a highly efficient electrode material can be expected. Feng *et al.* made use of the redox reaction between the outer skin of litchi and $KMnO_4$ to generate a large number of MnO_x nanoparticles on its surface, and then added melamine to successfully prepare 3D MnO@NLEFC. The mosaics of MnO nanoparticles increase the storage capacity of Li^+, significantly increase the carbon layer spacing and carbon disorder, and speed up the insertion and withdrawal of Li^+. Therefore, when applied to the anode of LIBs, the material still has a high reversible capacity of 515.5 mA h g^{-1} after 1000 cycles of 2 A g^{-1}.[169] In recent years, silica enriched biomass materials have been widely used in the preparation of high-performance silicon anodes.[170] Su *et al.* reported the conversion of maize leaves to silicon anode materials by a simple thermite reduction reaction. The obtained silicon material inherits the natural structure of the natural maize leaf and has a high porosity and amorphous/crystal mixture structure, providing a high capacity of 1200 mA h g^{-1} at a current density of 8 A g^{-1} and maintaining nearly 100% capacity after long-term cycling.[171]

Bird eggshells contain large amounts of calcium carbonate, which was reduced to calcium oxide through a thermochemical reaction and then treated by coating to prepare the nickel-rich cathode material $LiNi_{0.8}Co_{0.1}Mn_{0.1}O_2$ (NCM811) (Fig. 16B). The CaO layer effectively prevents electrolyte dissolution and electrode corrosion. Therefore, the NCM811 electrode coated with enough CaO (especially 1 wt%) has a discharge capacity of 177 mA h g^{-1} after 50 cycles, and the capacity retention rate is 92.6%, which is significantly better than that of bare NCM811 (82.9%).[172] Using waste reeds, Zhang *et al.* successfully constructed a beaded lithium vanadium phosphate/nanofiber carbon (LVP/NC) composite based on a nanocellulosic framework by the self-assembly method. After carbonization, a unique structure with LVP nanoparticles was embedded onto the porous carbon nanofibers, and when applied as a cathode for LIBs, a discharge specific capacity of 131.6 mA h g^{-1}, a capacity retention of 90% at 10 C after 1000 cycles and long-term cycling performance

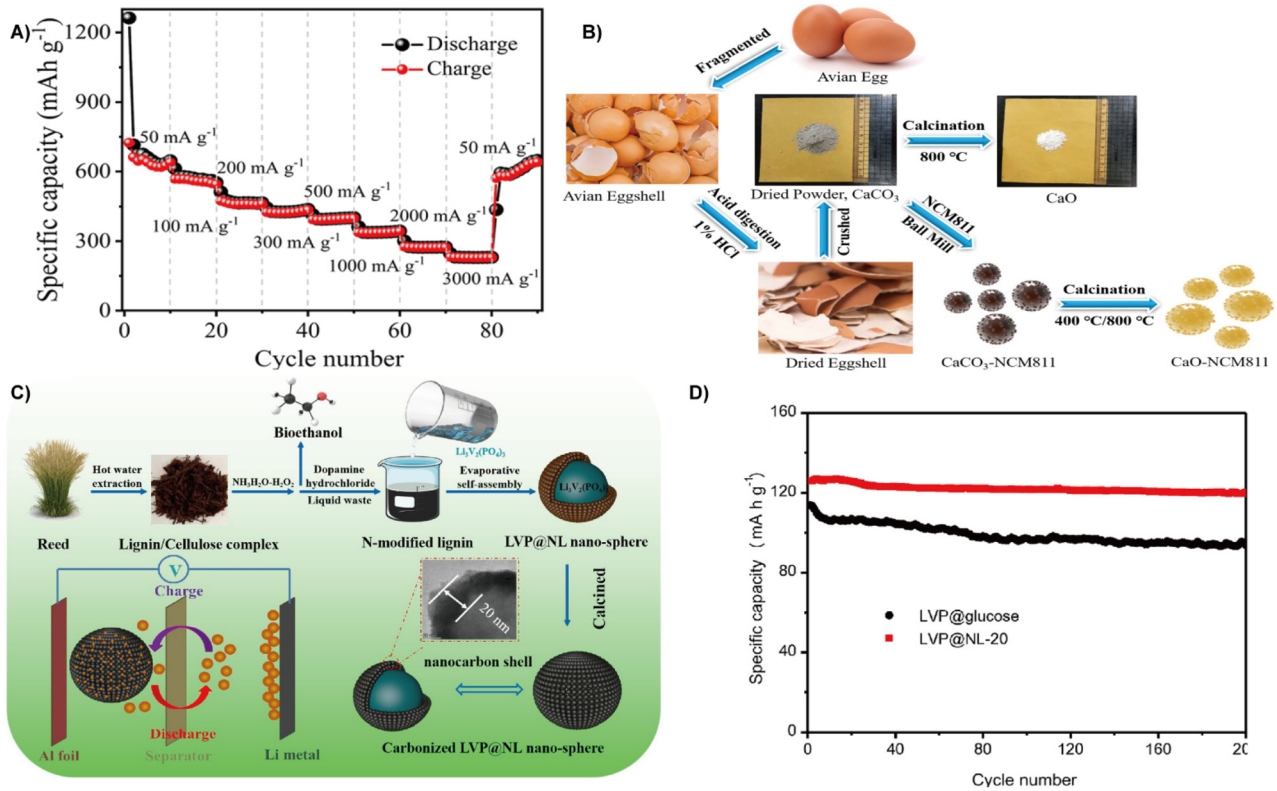

Fig. 16 (A) Cycling performance and coulombic efficiency.[21] Reprinted with permission. Copyright 2021, Springer. (B) Schematic illustration of the thermochemical conversion process of yielding a bio-derived material from eggshell and its coating over NCM8.[172] Reprinted with permission. Copyright 2019, Elsevier. (C) Schematic illustration of the fabrication process and proposed mechanism of the core–shell LVP@NL nanosphere. (D) Cycling performances of LVP@glucose and LVP@NL at 0.5C.[174] Reprinted with permission. Copyright 2022, Elsevier.

can be obtained.[173] Lignin from waste reed is also a potential energy source for cathode materials of batteries. Lu *et al.* immersed the lignin/cellulose mixture extracted from the waste reed into ammonia and hydrogen peroxide to obtain nitrogen-doped lignin, which is then treated with $Li_3V_2(PO_4)_3$ by self-assembly and carbonization to form a carbon coated LVP cathode material (carbonized LVP@NL nanospheres) (Fig. 16C). The carbon layers rich in oxygen-containing functional groups are favorable for promoting Li^+ kinetic behavior, therefore, displaying a high initial discharge capacity of 126.9 mA h g^{-1} at 0.5 C and maintaining the capacity retention of 88.9% at 10 C after 1000 cycles (Fig. 16D).[174]

4.2. Lithium–sulfur batteries (LSBs)

With higher theoretical specific capacity (1675 mA h g^{-1}) and energy density (2600 W h kg^{-1}), LSBs are emerging as a new class of rechargeable batteries.[175,176] The key problems restricting the application of LSBs are low sulfur utilization, poor long-term stability, large volumetric expansion, and low coulombic efficiency. Carbon materials with high electrical conductivity and a porous structure can not only improve conductivity, but also provide volume space for sulfur conversion to polysulfide.[177,178] Biomass derived carbon materials with porous structures and an abundance of surface functional groups are considered as effective cathode in batteries with higher specific capacity than conventional graphite materials.[122,179] For instance, rice hulls derived carbon was employed in the lithium metal anode and sulfur cathode in LSBs. Surface functionalization of rice husk derived carbon can effectively control lithium deposition, significantly decrease the nucleation overpotential, and improve the Coulombic efficiency. On the cathode side, rice husk derived carbon with a high specific surface area is conducive to limiting sulfur and sulfide. Therefore, the optimized LSBs have better discharge capacity and cycling stability with a capacity of 800 mA h^{-1} after 300 cycles.[180]

Biomass can also be transformed into functional scaffolds to obtaini cathode/anode materials with better performance and high stability.[181] At present, one of the problems of LSBs is the dissolution and migration of lithium polysulfide to the anode during cycling (*i.e.* the "shuttle effect"), which leads to the loss of active sulfur and the passivation of anode materials, and causes irreversible serious damage tocapacity of the battery.[182] Xiao *et al.* prepared a nitrogen-doped layered porous carbon (PCKH) from pomelo peels by carbonization and dual activation with the introduction of urea (Fig. 17A). The introduction of nitrogen increases the polarity of porous carbon and strengthens the strong polarity force interaction between carbon materials and lithium polysulfides, which effectively inhibits the shuttle effect.[183] Therefore, the PCKH

fabricated cathode in LSBs yielded an excellent initial capacity of 1534.6 mA h g^{-1} and a high Coulombic efficiency of over 98% at 300 cycles (Fig. 17B).[184] Unlike pomelo peels, which require the introduction of urea for nitrogen doping, nori, a naturally abundant alga, contains a large number of heteroatomic functional groups (nitrogen and oxygen) can achieve self-doping (Fig. 17C). Direct carbonization and subsequent activation of natural nori can yield activated nori carbon (ANC) for sulfur cathodes. When applied to LSBs, the nitrogen and oxygen dual-doped ANC cathode with a sulfur content of 81.2% reveals a good rate capacity over 5 C.[185]

Searching for a green and sustainable strategy for the production of scalable and cost effective sources is feasible to broaden the practical application in energy storage.[9,186] Taking advantage of the spent graphite, Xu and coworkers successfully exploited a spent graphite-based interlayer for LSB cathode materials from spent batteries (Fig. 17D). With the transition metals (such as Ni, Co, Mn) in the cathode material dissolved into the spent graphite, polysulfide can be adsorbed through S–TM bonds, improving the conductivity and promoting the conversion of polysulfide. As a result, the adsorption and catalytic performance of waste graphite on polysulfide are enhanced, suggesting a high discharge capacity of 968 mA h g^{-1} and a low decay rate of 0.08% at 1 C after 500 cycles.[13] Similarly, Yang *et al.* use spent graphite directly as a substrate for cathodes in LSBs. The large number of functional groups produced by repeated charge and discharge on a spent graphite surface and various metal elements produced by the dissolution of cathode materials can jointly improve the conductivity of lithium polysulfide (LiPS), effectively promote the transformation kinetics of LiPS and reduce the shuttle effect in LSBs. Thus, after 500 cycles, the cathode still has a high specific capacity of 765 mA h g^{-1} and an average decay rate of 0.006% per cycle at 0.5 C.[187] In addition, using waste PET bottles, Pietrzak *et al.* successfully prepared activated carbon with a large specific surface area and gradient pore structure through pyrolysis and K_2CO_3 activation. The gradient carbon provides a pathway for electron conduction, ensures good electrolyte accessibility, and facilitates the encapsulation of sulfur types and polysulfide lithium. The new active gradient carbon is particularly suitable for sulfur cathode in LSBs, showing a large initial specific discharge capacity of about 829 mA h g^{-1} at a current rate of 0.05 C, and the capacity retention rate is 86% after 50 cycles of charge and discharge.[188]

4.3. Lithium–oxygen batteries (LOBs)

LOBs have a 10 times higher theoretical energy density (3500 W h kg^{-1}) than LIBs, showing great prospects in energy conversion and storage.[189,190] However, one of the technical challenges of LOBs is the generation of the non-conductive and insoluble discharge product Li_2O_2, which results in limited active sites and sluggish kinetics of the charging process.[191]

Biomass derived carbon with a high specific surface area and electrical conductivity could act as a cathode, which favors

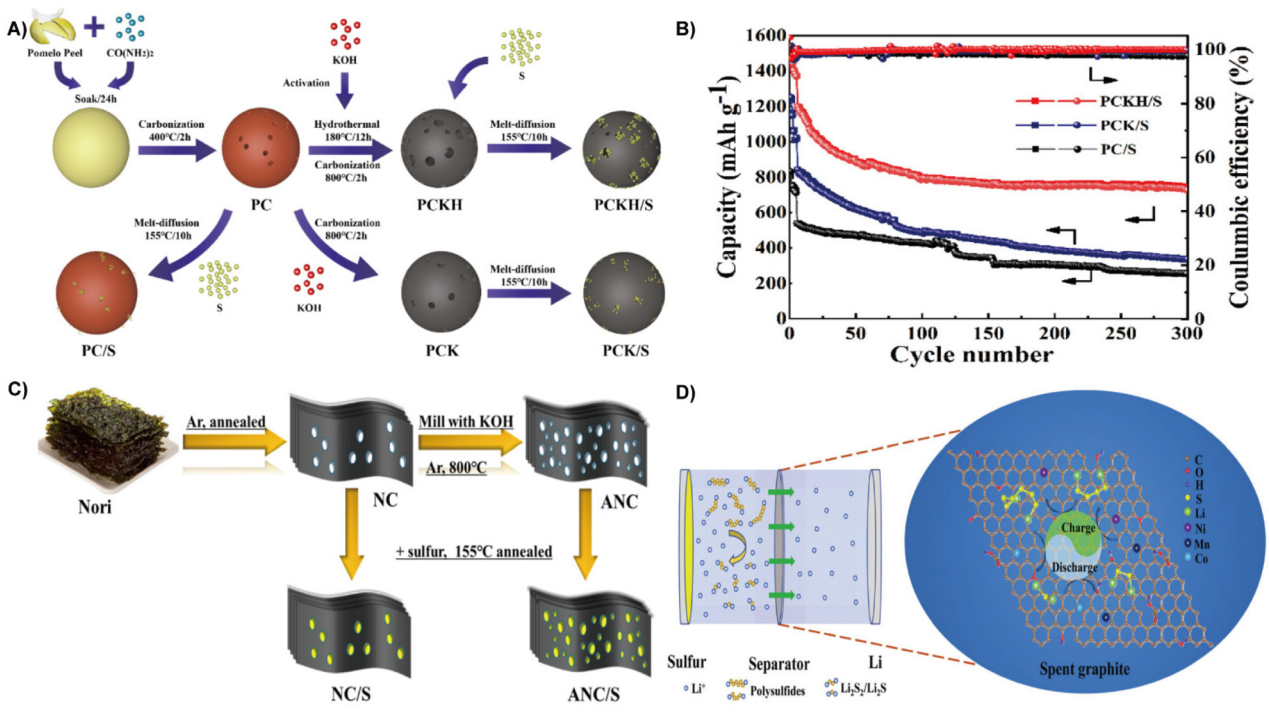

Fig. 17 (A) Schematic illustration of the synthesis process of porous carbon/sulfur composites. (B) Cycling performances of cells at 0.2 C with first 5 cycles at 0.1 C.[184] Reprinted with permission. Copyright 2020, Elsevier. (C) Synthesis scheme of 3D NC/S and ANC/S hybrids.[185] Reprinted with permission. Copyright 2017, American Chemical Society. (D) A schematic illustration of the adsorption properties and catalytic effects of an SG-modified separator in Li–S batteries.[13] Reprinted with permission. Copyright 2021, The Royal Society of Chemistry.

the Li_2O_2 decomposition and prompts facile mass transfer.[7,192] Li *et al.* used citrus peel (CMP) as a precursor to prepare activated carbon and iron-carrying carbon (CMPACs and CMPACs-Fe) through pyrolysis and KOH activation under nitrogen atmosphere. The introduction of Fe results in a lower overpotential of the O_2 electrode during charging and discharging. Thanks to the porous structure, abundant active sites and high specific surface area, CMPAC-based LOBs have a high specific capacity of 7800 mA h g^{-1} and are able to cycle 466 times while showing a high Coulombic efficiency of 92.5%.[193] Wang *et al.* prepared poplar inflorescences into self-nitrogen-doped activated carbons (N-PIACs) for LOBs by activation and slow pyrolytic carbonization. The 3D cross-linked pore structure of N-PIACs provides an effective buffer space for O_2/Li_2O_2 conversion and improves O_2 diffusion transfer. The excellent performance is reflected by the specific capacity of the Li/N-PIACs-O_2 battery (12 060 mA h g^{-1}), which is significantly higher than that of the original plant waste-based LOBs (N-PICs).[194] Similarly, Zhu *et al.* used apples to form N-doped graded porous active carbons (N-HMACs) through pyrolysis, and then used a solvothermal method to anchor RuO_2 nanoparticles on their surfaces to obtain N-HMACs-RuO_2 materials, as presented in Fig. 18A. When N-HMACs-RuO_2 was used directly as an air cathode for LOBs, the high specific surface area caused by the gradient porous architecture facilitates the transport of reactants and the sedimentation of discharge products, achieving a high discharge capacity of 1300 mA h g^{-1} and excellent long-term cycling stability (215 cycles, over 2000 h) (Fig. 18B).[195]

4.4. Other batteries (SIBs, KIBs, ZIBs, and ZABs)

Biomass based carbon possesses ideal open channels which serves as an ideal anode material for batteries.[20,196] For instance, rubber-wood sawdust was utilized as a source for the preparation of hierarchical porous hard carbon, which was then used as an anode material for SIBs (Fig. 19A). The as-synthesized hard carbon reveals a hierarchical porous structure with a specific surface area of 820 m^2 g^{-1}. The presence of porosity and oxygen functionalities promote the Na-ion storage sites.[197] In addition, a variety of biomass such as driftwood and fruit peels, or marine based shrimp rich in highly electronegative elements (oxygen, carbon, sulfur and nitrogen) have also been developed for SIBs.[198–200]

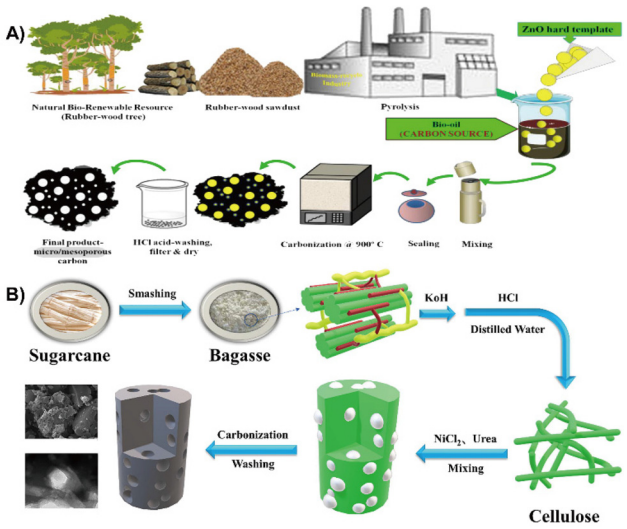

Fig. 19 (A) Schematic designs of resource collection and synthesis route of hierarchical porous hard carbon.[197] Reprinted with permission. Copyright 2019, Elsevier. (B) Flow chart of as-synthesized biomass porous carbon materials.[201] Reprinted with permission. Copyright 2021, Elsevier.

The bagasse biomass waste was utilized to develop a nitrogen doped 3D porous carbon material through carbonization and further treatment with $NiCl_2$ and urea, which was used as an advanced anode material for KIBs (Fig. 19B). The results show that $NiCl_2$ promotes the formation of porous structures and nitrogen doping allows morphological changes which enables rapid K^+ and electron transport. More importantly, the material exhibits outstanding K^+ storage performance, with a reversible capacity of 100.4 mA h g^{-1} at a current density of 200 mA g^{-1} for 400 cycles without significant capacity decay.[201] Besides, common biomass such as potato and

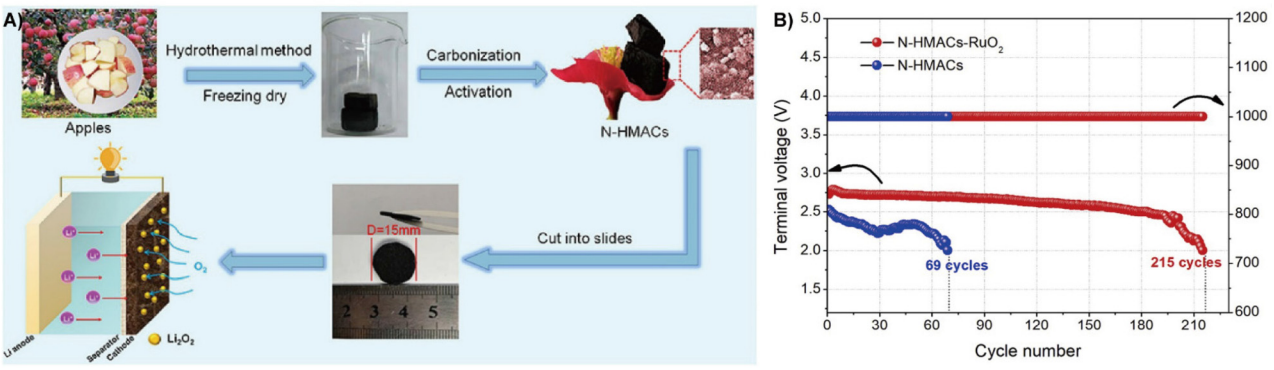

Fig. 18 (A) The synthesis strategy of N-HMACs and the construction of a Li–O_2 battery with an N-HMAC cathode. (B) Voltage of the terminal discharge and the cycle number.[195] Reprinted with permission. Copyright 2020, Elsevier.

walnut septum are also transfered into anode materials for KIBs.[202,203]

ZIBs and ZABs have received attention because of their non-flammable, abundant zinc resources (~300 times higher than lithium).[204] The active metals in spent catalysts which are hazardous waste can be converted to valuable materials for ZIBs and ZABs. Spent hydrogenation catalysts with vanadium are easily recovered through hydrothermal treatment to prepare graded hydrated vanadium oxides (HVOs) as cathode materials for ZIBs. The layered spherical $V_{10}O_{22.8}{\cdot}12H_2O$ achieved discharge specific capacity values of 287 mA h g^{-1} and 238 mA h g^{-1} at 0.2 A g^{-1} and 1 A g^{-1}, respectively. In addition, a high energy density of 106 W h kg^{-1} at a power density of 3324 W kg^{-1} and a capacity retention of 82% after 3000 cycles at a high density of 10 A g^{-1} can be obtained (Fig. 20A and B).[205] The recovery of NiCoMn from spent batteries has also been transferred to efficient electrode materials in ZABs. Jiao *et al.* reported the conversion of $LiNi_{1-x-y}Mn_xCo_yO_2$ (NMC) cathodes of spent LIBs to NiMnCo-based catalysts for ZAB cathodes using a fast thermal radiation method. The NiMnCo-AC electrocatalyst in the cathode has a low voltage gap of 0.72 V for the first three cycles, exhibits a high power density of 187.7 mW cm^{-2} and a long cycling duration (Fig. 20C and D).[206]

4.5. Supercapacitors

Of all the energy storage devices, supercapacitors feature better cycling stability, high power density, and excellent conductivity.[6,207] However, the low energy density of supercapacitors has severely limited their widespread use, prompting researchers to develop new electrode materials.[208] The energy density is proportional to the specific capacitance, which differs by electrode materials. Noble metal oxides are recognized as ideal electrode materials with high specific capacitance, but their scarcity and high cost limit their wide application. Biomass-derived carbon with a high specific surface area, graded porous structure, and hydrophilic surface functional groups enables excellent electrical conductivity and pseudocapacity. However, these materials are widely available in waste, and reusing these waste materials could solve the problem encountered in the preparation of electrode materials in supercapacitors.[209] Therefore, the following section describes the reuse of waste to electrode materials for supercapacitors.

Spent batteries for supercapacitors. Spent batteries with rich metals have been disposed and cause severe environmental problems, therefore, transferring the valuable metals to new electrode materials in an economical way is a critical task.[14] For instance, a cost-effective strategy for fabricating supercapacitor materials from spent LIBs has been reported by reorganizing cobalt, manganese and graphene in spent batteries for supercapacitor.[210] Barbieri *et al.* found out that the addition of KOH to the cathode solution of spent LIBs could lead to the recovery of cobalt by chemical and electrochemical precipitation to obtain $Co(OH)_2$, and then subsequent calcination in air directly produces the final product Co_3O_4, exhibiting a specific capacitance of 13.0 F g^{-1} (1.0 mV s^{-1}).[211] Furthermore, graphene is one of the excellent nano-functional fillers for supercapacitor composite electrodes.[212] Duan *et al.* used manganese dioxide from spent battery powder as an oxidant and graphene oxide as a 2D conductive carrier, followed by chemical oxidation polymerization with aniline and reduction with hydrazine hydrate to construct ternary composites (reduced graphene oxide/graphite nanoparticles/polyani-

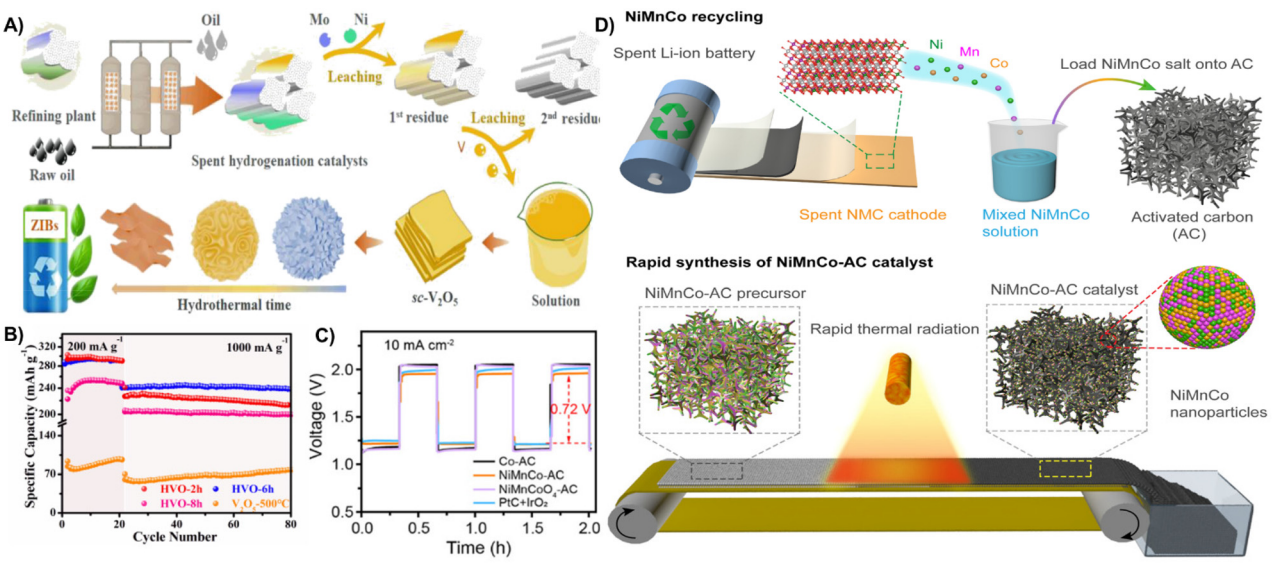

Fig. 20 (A) Schematic diagram of the fabrication process of hydrated vanadium oxides derived from spent hydrogenation catalysts. (B) Cycling performance at 0.2 A g^{-1} and 1 A g^{-1}.[205] Reprinted with permission. Copyright 2022, Elsevier. (C) The initial three charge–discharge curves of ZABs at a current density of 10 mA cm^{-2}. (D) Schematic of the fabrication process of the NiMnCo-AC catalyst from spent LIBs.[206] Reprinted with permission. Copyright 2022, PANS.

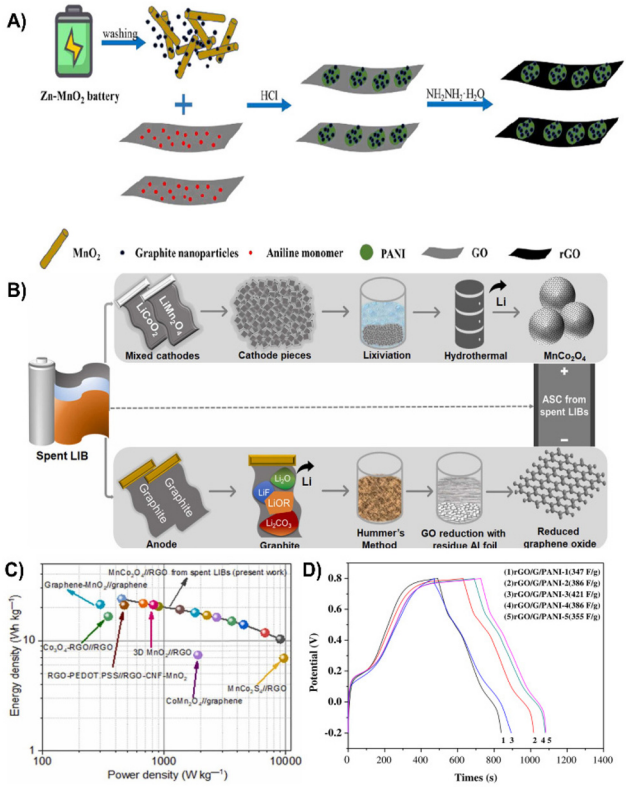

Fig. 21 (A) Complete recycling process and synthesis steps of the TRGNs–MoS_2 nanohybrid.[213] Reprinted with permission. Copyright 2017, Elsevier. (B) Schematic representation for the fabrication of an asymmetric supercapacitor from spent LIB components. (C) Ragone plot of the device from the regenerated spent LIB electrodes.[214] Reprinted with permission. Copyright 2022, Elsevier. (D) Comparison of specific capacitance at different scan rates for TRGNs-MoS_2.[215] Reprinted with permission. Copyright 2022, American Chemical Society.

line) as electrode materials for supercapacitors (Fig. 21A). Because of the strong π–π interaction between the three materials, the electrodes exhibited a capacitance of 421 F g^{-1} and a capacitance retention of 106.6% after 10 000 cycles.[213]

Recycling graphite from spent batteries is also one of the hot spots. Natarajan *et al.* regenerated 3D-$MnCo_2O_4$ (MCO) spheres from spent LIBs *via* the hydrothermal technique and converted anode graphite into reduced graphene oxide (rGO) by a facile Hummers acid oxidation method (Fig. 21B). The microsphere shape of MCO avoids self-aggregation after long-term cycling while rGO enables the high conductivity of the composite, and therefore, the composite based supercapacitor exhibits an operational voltage of 1.8 V and a large energy density of ~23.9 W h kg^{-1} at 450 W kg^{-1} with 8000 cycles (Fig. 21C).[214] In addition, Kishore *et al.* converted graphite in spent batteries into graphene nanosheets by acid leaching and calcination treatment, which was subsequently treated with MoS_2 to produce a nanocomplex. Due to the abundance of MoS_2 active sites and high conductivity of graphene nanosheets, the prepared composite electrode displayed a specific capacitance of 415 F g^{-1} (Fig. 21D).[215]

Biomass for supercapacitors. The preparation of high-performance supercapacitors from biomass-derived carbon can overcome high manufacturing costs.[216,217] Biomass-derived carbon materials usually contain a large number of hydroxyl, carbonyl and carboxyl oxygen-containing functional groups, which can be applied in supercapacitors to prevent the oxidation of carbon and improve the cycling stability.[122] Moreover, biomass-derived carbon materials have good microporosity and enhanced electrical conductivity.[218,219] Li *et al.* prepared 3D layered porous carbon nanosheets by direct calcination of forestry waste bark and $CuBr_2$ (Fig. 22A). The copper salt has an activation effect and retains the original structure of biomass with a specific surface area up to 2396 m^2 g^{-1}. Therefore, it shows excellent capacity as a supercapacitor with a specific capacitance of 345.9 F g^{-1} at 0.5 A g^{-1} and a superior capacitance retention of 98.3% after 10 000 charge/discharge cycles.[220] KOH is one of the commonly used activators for biomass-derived carbon, which has strong pore-forming ability.[221] Kapok flower containing oxygen functional groups was treated by carbonization and KOH activation to prepare porous activated carbon with a specific surface area of 1904.1 cm^2 g^{-1}. The large specific surface area and excellent porosity enable a specific capacitance of 286.8 F g^{-1} at 1 A g^{-1} and a capacitance retention of up to 97.4% after 5000 cycles.[222]

In addition, waste corn stover powder was utilized to prepare hydrothermal carbon (HTC) layers on carbon fibers (CFs) by a hydrothermal reaction. Then, the gas generated from the pyrolysis of waste corn stover was introduced to generate carbon nanorods (CNRs) to form CNR/HTC/CFs by a gas-phase growth process (Fig. 22B). The presence of hollow fractures induces a high specific surface area and exhibits a high specific capacitance of 269.47 F g^{-1}.[219] Moreover, Subhani *et al.* converted chicken claws into interconnected porous collagen sponge by freeze-drying, and then coated with graphene nanosheets to obtain 3D porous carbon (Fig. 22C). The porous structure has a high specific surface area and increased ion diffusion channels, resulting in a specific capacitance of 365 F g^{-1} and excellent capacity retention of 97% after 10 000 cycles (Fig. 22D).[223] This section shows that waste natural plant wastes (*e.g.*, bark, corn stover) with large specific surface areas can be utilized as activated carbon by simple carbonization and activation methods which play an important role in the capacitance and stability of supercapacitors.

Other wastes for supercapacitors. Industrial waste contains valuable metals or precursors can be transferred into electrode materials for supercapacitors through different synthetic strategies. Considering electrical cable wires are composed of copper and aluminum, Nagaraju *et al.* employed discarded cables to prepare nickel oxide nanosheet grafted carbon nanotube coupled copper oxide nanowire arrays (NiO NSs@CNTs@CuO NWAs) by the wet-chemical method (Fig. 23A). Due to the vertical alignment of CuO NWAs and CNTs, the electrical conductivity was enhanced, and the accessible area for electrolyte penetration was increased, and therefore, the solid-state fiber-based hybrid supercapacitor as the

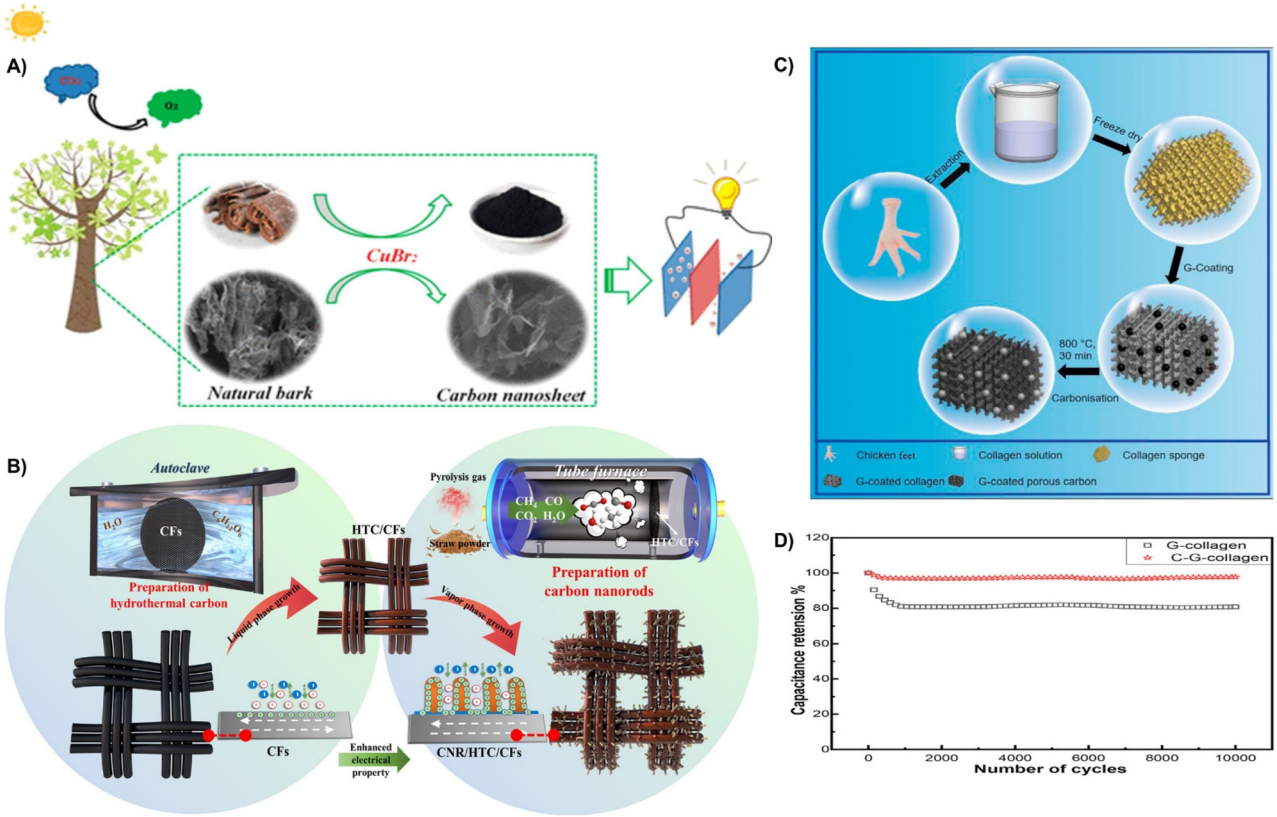

Fig. 22 (A) Preparation of the 3D porous carbon nanosheet.[220] Reprinted with permission. Copyright 2019, American Chemical Society. (B) The schematic diagram of the synthesis of CNR/HTC/CFs.[219] Reprinted with permission. Copyright 2021, Elsevier. (C) Schematic demonstration of collagen, G-collagen, and C-G-collagen fabrication. (D) Cyclic study of C-G-collagen.[223] Reprinted with permission. Copyright 2022, Elsevier.

positive electrode delivered the energy densities of 26.32 W h kg^{-1} and 1218.33 W kg^{-1}.[224]

Spent catalysts with valuable metals can be utilized as electrode materials, which reduce environmental pollution and shows excellent economic benefits.[225] Krishnamoorthy *et al.* effectively reused waste carbon-deposited siloxane/nickel catalysts by removing the Ca atoms and oxidizing the silicon layer present in $CaSi_2$ to form 2D siloxene sheets as electrodes for supercapacitors. Because of the high surface area, the supercapacitors prepared from spent catalysts delivered a high capacity of 24.65 F g^{-1}, an energy density of 30.81 W h kg^{-1}, and a power density of 15 625 W kg^{-1} (Fig. 23B).[226] Lim *et al.* proposed a strategy to transfer spent catalysts to Cu-loaded activated carbon fibers (Cu/ACFs) by chemical deposition, which deactivates Cu to CuO (CuO/ACF) during the process of nitric oxide removal. The spent catalysts were screened for direct application as electrode materials for supercapacitors with a specific capacitance of 74.7 F g^{-1} at 10 mA cm^{-2}.[227]

Moreover, the explosive amount of waste plastic caused serious environmental pollution due to the difficulty in degradation, and direct utilization could solve the conundrum.[11] For example, Zhang *et al.* successfully prepared activated carbon by pressure pyrolysis and post-activation from waste PET materials. The activated materials displayed a specific surface area of 2683 m^2 g^{-1} and rich surface functional groups. When used as supercapacitor electrodes, the specific capacitance reached a value of 325 F g^{-1}.[228] Besides, Ma *et al.* proposed a strategy by using Fe_2O_3 particles as a template and catalyst to transfer polystyrene (PS) to 3D hierarchical porous carbon under KOH activation (Fig. 23C). The template and KOH activation can generate well-balanced micro-, meso-, and macroporous structures, resulting in a high specific surface area (2100 m^2 g^{-1}). The synergistic effects contribute to a specific capacitance of 284.1 F g^{-1} at 0.5A g^{-1}, an energy density of 19.2 W h kg^{-1}, a power density of 200.7 W kg^{-1} as well as good rate performance and cycling stability (Fig. 23D).[229]

Besides, the increasing consumption of automobiles will generate a large amount of waste oil, which can be converted into activated carbon.[230] Kaipannan *et al.* successfully prepared porous activated carbon/ZnS composites (ACZS) by calcining waste engine oil under Ar atmosphere and acid treatment. The as-resulted ACZS displayed a surface area of 1020 m^2 g^{-1} and multiple micropores and mesopores, and delivered a specific capacitance of 240 F g^{-1} at 1 A g^{-1} and a capacity retention of 95% after 10 000 cycles.[231]

In the field of waste to wealth in energy storage, spent batteries, biomass, silicon and plastics are the main available waste materials. The cathode in waste LIBs contains active metal which can be reutilized through calcination and wet

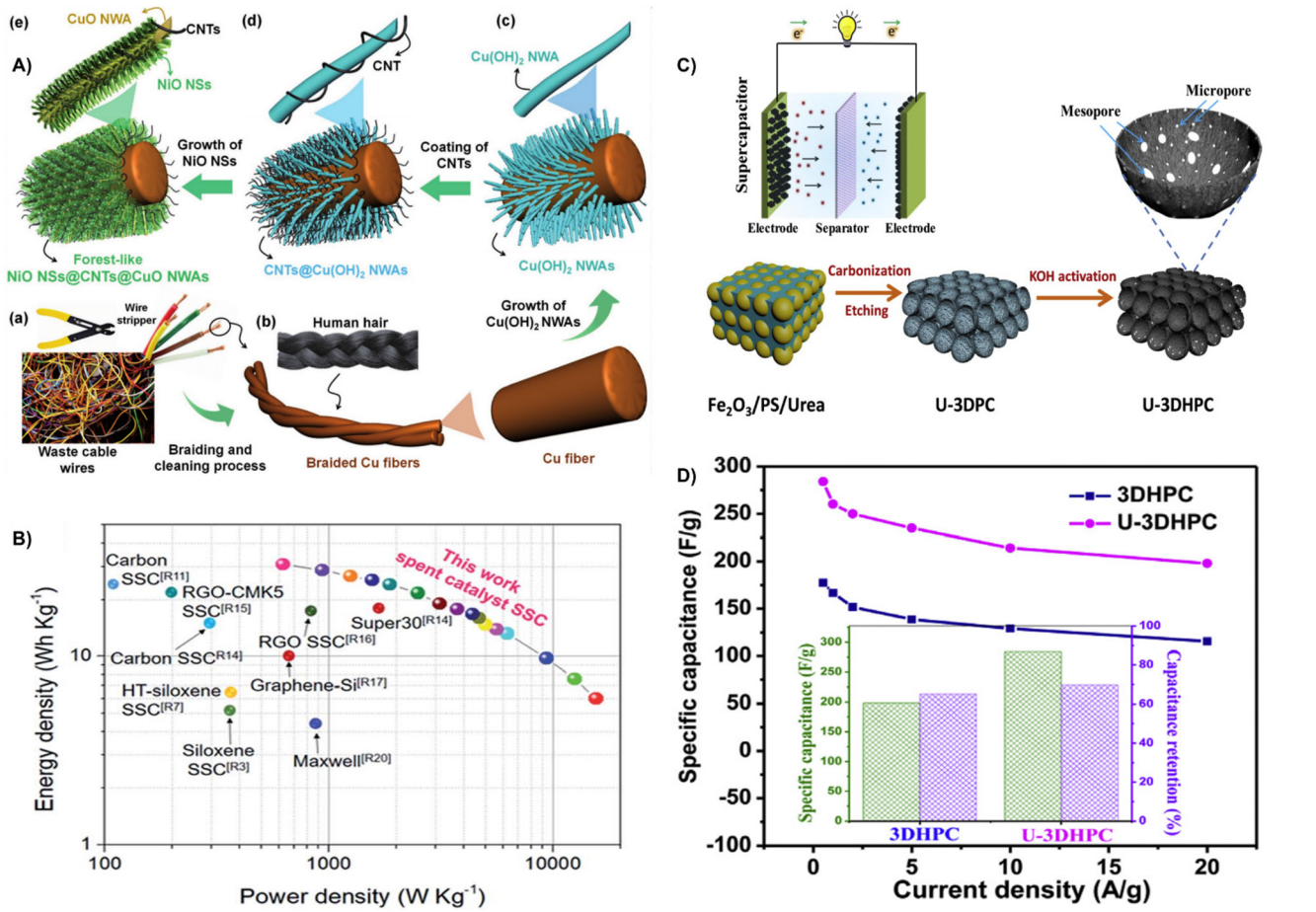

Fig. 23 (A) Schematic illustration showing the fabrication process of forest-like NiO NSs@CNTs@CuO NWAs/Cu fibers using waste cable wires.[224] Reprinted with permission. Copyright 2022, Wiley-VCH. (B) Ragone plot of the carbon/siloxene/Ni supercapacitor.[226] Reprinted with permission. Copyright 2019, The Royal Society of Chemistry. (C) Schematic illustration of the synthetic process for the preparation of 3D hierarchically porous carbon. (D) Specific capacitances of 3DHPC and U-3DHPC at 0.5–20 A g^{-1}; the inset indicates the specific capacitance of 0.5 A g^{-1} and capacitance retention at 20 A g^{-1}.[229] Reprinted with permission. Copyright 2020, Elsevier.

chemical treatment to construct electrocatalysts and electrode materials. Biomass, plastic and anode of spent batteries can be converted into large specific surface area and porous carbon materials by calcination and microwave irradiation. However, the synthesis of biomass and plastic derived carbon is still on the laboratory scale and needs to be further explored in large scale production. Silicon from waste glass and waste photovoltaic panels can be converted into nanosilicon for electrodes in LIBs, but the preparation requires high-precision equipment and strictly controlled parameters. In face of growing demands for energy storage systems, the waste to treasure strategy provides a sustainable and economical way to develop highly efficient electrode materials.

5. Conclusion

Transforming waste into electrocatalysts and electrode materials is of vital importance to achieve carbon neutrality. This review classifies and summarizes the recent advances in the conversion and application of waste materials in green sustainable energy, emphasizing on the waste category and reutilization strategies, especially highlighting the recent progress in electrocatalysis applications (HER, OER, ORR, CO_2RR and NRR) and energy conversion and storage systems (LIBs, LSBs, LOBs, SIBs, KIBs, ZIBs, ZABs and supercapacitors).

The direct conversion to electrocatalysts and energy storage materials can be performed either from waste materials alone or in combination with other commercial components. We note that spent batteries rich in active metallics are widely used as excellent HER, OER and ORR electrocatalysts, while spent graphite is easily transformed into a carbon material as a substrate for electrocatalysts and electrode anode materials in batteries and supercapacitors. Biomass derived carbon has the advantages of low cost, green synthesis, easy accessibility, and compliance with sustainable development strategies, which can alleviate the huge demand for synthetic carbon materials. The direct transformation of biomass by pyrolysis, hydrothermal methods, and carbonization in the presence of an activator led to the realization of porous structures and abundant surface functional groups, resulting in an increased electron transfer rate and enhanced specific capacity. Plastic

waste with synthetic polymers and municipal sludge rich in heteroatoms (P, N and S) are used as a cost-effective and readily available precursor for the preparation of carbon substrates for electrocatalysts. Industrial wastewater rich in reactive metals (Cu and Pb) favours the CO_2RR. In addition, a large number of metals (large amounts of Si, Ni, Cu, Sn, Fe, Al and Ag and trace amounts of Pb, Sb, Pd and Cr) in industrial treated waste catalysts can be employed to prepare various electrocatalysts and electrode materials.

Although waste utilization is promising in terms of environmental protection and sustainable development, there are still some drawbacks and challenges that hinder practical applications. Firstly, spent batteries are complex in composition and contain unknown impurity elements and compounds. To improve the product quality, additional treatment is usually required to remove the impurity elements, which complicate the treatment. Secondly, compared to commercially available carbon, biomass based carbon lacks flexibility and is difficult to complex with a wide range of functional materials to further improve the electrochemical performance. Thirdly, the synthetic strategy and characterization technique are highly sensitive to varied waste sources from different locations, and therefore, a stable waste source, reduced cost and contamination issues are required for the industrial production of these waste to wealth materials.

In summary, the "Waste to Wealth" strategy could directly convert waste materials into electrocatalysts and energy storage materials in an eco-friendly and energy conservation manner. It not only provides a straightforward way to solve the energy and environmental crisis by reducing undesirable waste hazards to the environment, but also paves a new way for the large-scale production of electrocatalysts and electrode materials for electrocatalysis and energy storage.

Author contributions

Chengcheng Yan: Conceptualization, data curation, investigation, and writing – original draft; Xun Jiang: data curation, investigation, and writing – original draft; Jiaxin Yu: data curation, investigation, and writing; Zhaolong Ding: data curation, investigation, and writing; Ling Ma: data curation; Tingyu Su: data curation; Yilu Wang: data curation; Chunxia Wang: conceptualization and writing – review & editing; Guoyong Huang: funding acquisition and writing – review & editing; and Shengming Xu: supervision.

Conflicts of interest

There are no conflicts to declare.

Acknowledgements

This project was supported by National Key Research and Development Program of China (No. 2021YFC2901100), the National Natural Science Foundation of China (No. 52022109, 51834008, 52274307 and No. 21804319), Science Foundation of China University of Petroleum, Beijing (No. 2462022QZDX008, 2462021QNX2010, 2462020YXZZ019 and 2462020YXZZ016), State Key Laboratory of Heavy Oil Processing (HON-KFKT2022-10).

References

1 Y. Wang, H. Su, Y. He, L. Li, S. Zhu, H. Shen, P. Xie, X. Fu, G. Zhou and C. Feng, *Chem. Rev.*, 2020, **120**, 12217–12314.
2 Z. W. Seh, J. Kibsgaard, C. F. Dickens, I. Chorkendorff, J. K. Nørskov and T. F. Jaramillo, *Science*, 2017, **355**, eaad4998.
3 Y. Li, H. Wang, C. Priest, S. Li, P. Xu and G. Wu, *Adv. Mater.*, 2021, **33**, 2000381.
4 J. Li, J. Fleetwood, W. B. Hawley and W. Kays, *Chem. Rev.*, 2021, **122**, 903–956.
5 Y. Zhou, Q. Han, Y. Liu, Y. Wang, F. Jiang, N. Wang, Z. Bai and S. Dou, *Energy Storage Mater.*, 2022, **5**, 308–333.
6 Y. Zhou, H. Qi, J. Yang, Z. Bo, F. Huang, M. S. Islam, X. Lu, L. Dai, R. Amal and C. H. Wang, *Energy Environ. Sci.*, 2021, **14**, 1854–1896.
7 S. Park, J. Kim and K. Kwon, *Chem. Eng. J.*, 2022, **446**, 137116.
8 D. J. Garole, R. Hossain, V. J. Garole, V. Sahajwalla, J. Nerkar and D. P. Dubal, *ChemSusChem*, 2020, **13**, 3079–3100.
9 S. Natarajan and V. Aravindan, *Adv. Energy Mater.*, 2018, **8**, 1802303.
10 S. Abdolhosseinzadeh, R. Schneider, A. Verma, J. Heier, F. Nüesch and C. Zhang, *Adv. Mater.*, 2020, **32**, 2000716.
11 X. Zhao, M. Korey, K. Li, K. Copenhaver, H. Tekinalp, S. Celik, K. Kalaitzidou, R. Ruan, A. J. Ragauskas and S. Ozcan, *Chem. Eng. J.*, 2022, **428**, 131928.
12 X. Zhang, L. Li, E. Fan, Q. Xue, Y. Bian, F. Wu and R. Chen, *Chem. Soc. Rev.*, 2018, **47**, 7239–7302.
13 Q. Xu, Y. Wang, X. Shi, Y. Zhong, Z. Wu, Y. Song, G. Wang, Y. Liu, B. Zhong and X. Guo, *Green Chem.*, 2021, **23**, 942–950.
14 D. Ruan, K. Zou, K. Du, F. Wang, L. Wu, Z. Zhang, X. Wu and G. Hu, *ChemCatChem*, 2021, **13**, 2025–2033.
15 J. Wang, J. Ma, K. Jia, Z. Liang, G. Ji, Y. Zhao, B. Li, G. Zhou and H.-M. Cheng, *ACS Energy Lett.*, 2022, **7**, 2816–2824.
16 J. J. Roy, S. Rarotra, V. Krikstolaityte, K. W. Zhuoran, Y. D. I. Cindy, X. Y. Tan, M. Carboni, D. Meyer, Q. Yan and M. Srinivasan, *Adv. Mater.*, 2022, **34**, 2103346.
17 S. Natarajan and V. Aravindan, *Adv. Energy Mater.*, 2020, **10**, 2002238.
18 S. Natarajan, M. L. Divya and V. Aravindan, *J. Energy Chem.*, 2022, **71**, 351–369.
19 W. Chen, R. V. Salvatierra, J. T. Li, C. Kittrell, J. L. Beckham, K. M. Wyss, N. La, P. E. Savas, C. Ge and P. A. Advincula, *Adv. Mater.*, 2022, 2207303.

20 X. Yuan, B. Zhu, J. Feng, C. Wang, X. Cai and R. Qin, *Chem. Eng. J.*, 2021, **405**, 126897.
21 X. Chen, F. Li, S. Su, H. Chen, J. Zhang and D. Cai, *Environ. Chem. Lett.*, 2021, **19**, 3505–3510.
22 C. Senthil and C. W. Lee, *Renewable Sustainable Energy Rev.*, 2021, **137**, 110464.
23 W. Long, B. Fang, A. Ignaszak, Z. Wu, Y.-J. Wang and D. Wilkinson, *Chem. Soc. Rev.*, 2017, **46**, 7176–7190.
24 J. Wei, Y. Liang, Y. Hu, B. Kong, G. P. Simon, J. Zhang, S. P. Jiang and H. Wang, *Angew. Chem., Int. Ed.*, 2016, **55**, 1355–1359.
25 V. R. Jothi, R. Bose, H. Rajan, C. Jung and S. C. Yi, *Adv. Energy Mater.*, 2018, **8**, 1802615.
26 Y. Yang, H. Yang, H. Cao, Z. Wang, C. Liu, Y. Sun, H. Zhao, Y. Zhang and Z. Sun, *J. Cleaner Prod.*, 2019, **236**, 117576.
27 H. Guven, R. K. Dereli, H. Ozgun, M. E. Ersahin and I. Ozturk, *Energy Combust. Sci.*, 2019, **70**, 145–168.
28 L. Deng, H. Yuan, X. Qian, Q. Lu, L. Wang, H. Hu and Y. Chen, *Resour., Conserv. Recycl.*, 2022, **177**, 105980.
29 Q. Yue and L. Luo, *Chem*, 2022, **8**, 2326–2329.
30 K. Zheng, Y. Wu, Z. Hu, S. Wang, X. Jiao, J. Zhu, Y. Sun and Y. Xie, *Chem. Soc. Rev.*, 2023, **52**, 8–29.
31 V. R. Jothi, K. Karuppasamy, T. Maiyalagan, H. Rajan, C. Y. Jung and S. C. Yi, *Adv. Energy Mater.*, 2020, **10**, 1904020.
32 F. Xi, Z. Zhang, Y. Hu, S. Li, W. Ma, X. Chen, X. Wan, C. Chong, B. Luo and L. Wang, *J. Hazard. Mater.*, 2021, **414**, 125480.
33 S. Yang, H. An, D. Anastasiadou, W. Xu, L. Wu, H. Wang, J. de Ruiter, S. Arnouts, M. C. Figueiredo and S. Bals, *ChemCatChem*, 2022, **14**, e202200754.
34 C. Jin, J. Nai, O. Sheng, H. Yuan, W. Zhang, X. Tao and X. W. D. Lou, *Energy Environ. Sci.*, 2021, **14**, 1326–1379.
35 P. Liu, Y. Wang and J. Liu, *J. Energy Chem.*, 2019, **34**, 171–185.
36 Z. Chen, W. Wei, H. Chen and B.-J. Ni, *Int. J. Hydrogen Energy*, 2023, **48**, 6288–6307.
37 Y. Sun, Y. Zang, W. Tian, X. Yu, J. Qi, L. Chen, X. Liu and H. Qiu, *Energy Environ. Sci.*, 2022, **15**, 1201–1210.
38 A. Eftekhari, *Int. J. Hydrogen Energy*, 2017, **42**, 11053–11077.
39 Y. Shen, *J. Power Sources*, 2022, **528**, 231220.
40 T. Liu, S. Cai, G. Zhao, Z. Gao, S. Liu, H. Li, L. Chen, M. Li, X. Yang and H. Guo, *J. Energy Chem.*, 2021, **62**, 440–450.
41 X. Zheng, X. Zhao, J. Lu, J. Li, Z. Miao, W. Xu, Y. Deng and A. L. Rogach, *Sci. China Mater.*, 2022, **65**, 1–8.
42 J. He, Z. Wu, Q. Gu, Y. Liu, S. Chu, S. Chen, Y. Zhang, B. Yang, T. Chen and A. Wang, *Angew. Chem.*, 2021, **133**, 23906–23914.
43 J. Sun, Z. Wu, C. Ma, M. Xu, S. Luo, W. Li and S. Liu, *J. Mater. Chem. A*, 2021, **9**, 13822–13850.
44 W. Zhang, R. Xi, Y. Li, Y. Zhang, P. Wang and D. Hu, *Int. J. Hydrogen Energy*, 2022, **47**, 32436–32454.
45 Z. Zhang, S. Yang, H. Li, Y. Zan, X. Li, Y. Zhu, M. Dou and F. Wang, *Adv. Mater.*, 2019, **31**, 1805718.
46 O. A. Fakayode, B. A. Yusuf, C. Zhou, Y. Xu, Q. Ji, J. Xie and H. Ma, *Energy Convers. Manage.*, 2021, **227**, 113628.
47 R. Zhang, X. Du, S. Li, J. Guan, Y. Fang, X. Li, Y. Dai and M. Zhang, *J. Electroanal. Chem.*, 2022, **921**, 116679.
48 W. Zhang, R. Xi, Y. Li, Y. Zhang, P. Wang and D. Hu, *Colloids Surf., A*, 2023, **658**, 130704.
49 Y. Liu, G. Mou, Y. Wang, F. He, N. Dong, Y. Lin, M. Zhong and B. Su, *ACS Appl. Nano Mater.*, 2022, **5**, 2953–2961.
50 V. G. Gomes and K. N. Dinh, *Electrochim. Acta*, 2019, **314**, 49–60.
51 S. Min, Y. Duan, Y. Li and F. Wang, *Renewable Energy*, 2020, **155**, 447–455.
52 S. Hong, N. Song, E. Jiang, J. Sun, G. Chen, C. Li, Y. Liu and H. Dong, *J. Colloid Interface Sci.*, 2022, **608**, 1441–1448.
53 W. Yaseen, M. Xie, B. A. Yusuf, Y. Xu, M. Rafiq, N. Ullah, P. Zhou, X. Li and J. Xie, *Int. J. Hydrogen Energy*, 2022, **47**, 15673–15686.
54 S. Sekar, A. T. A. Ahmed, D. H. Sim and S. Lee, *Int. J. Hydrogen Energy*, 2022, **47**, 40317–40326.
55 J. Joyner, E. F. Oliveira, H. Yamaguchi, K. Kato, S. Vinod, D. S. Galvao, D. Salpekar, S. Roy, U. Martinez and C. S. Tiwary, *ACS Appl. Mater. Interfaces*, 2020, **12**, 12629–12638.
56 Y. Gu, B. Xi, R. Wei, Q. Fu, Y. Qain and S. Xiong, *Nano Lett.*, 2020, **20**, 8375–8383.
57 Z. Sun, D. K. James and J. M. Tour, *J. Phys. Chem. Lett.*, 2011, **2**, 2425–2432.
58 F. He, Y. Han, Y. Tong, M. Zhong, Q. Wang, B. Su and Z. Lei, *ACS Sustainable Chem. Eng.*, 2022, **10**, 6094–6105.
59 H.-F. Wang, L. Chen, H. Pang, S. Kaskel and Q. Xu, *Chem. Soc. Rev.*, 2020, **49**, 1414–1448.
60 K. Gravouil, R. Ferru-Clément, S. Colas, R. Helye, L. Kadri, L. Bourdeau, B. Moumen, A. Mercier and T. Ferreira, *Environ. Sci. Technol.*, 2017, **51**, 5172–5181.
61 M. Ubaidullah, A. M. Al-Enizi, S. Shaikh, M. A. Ghanem and R. S. Mane, *J. King Saud Univ., Sci.*, 2020, **32**, 2397–2405.
62 L. Gao, F. Zhou, Q. Chen and G. Duan, *ChemistrySelect*, 2018, **3**, 5321–5325.
63 R. A. Mir and O. Pandey, *J. Cleaner Prod.*, 2019, **218**, 644–655.
64 X. Han, N. Lin, M. Chen, Z. Wang, Y. Tang and C. Ma, *Scr. Mater.*, 2021, **204**, 114159.
65 A. Wu, A. Xu, J. Yang, X. Li, L. Wang, J. Wang, D. Macdonald and J. Yan, *ChemElectroChem*, 2018, **5**, 3841–3846.
66 Z. Chen, W. Wei, W. Zou, J. Li, R. Zheng, W. Wei, B.-J. Ni and H. Chen, *Green Chem.*, 2022, **24**, 3208–3217.
67 G. Righi, J. Plescher, F.-P. Schmidt, R. K. Campen, S. Fabris, A. Knop-Gericke, R. Schlögl, T. E. Jones, D. Teschner and S. Piccinin, *Nat. Catal.*, 2022, **5**, 888–899.
68 D. Du, Z. Zhu, K.-Y. Chan, F. Li and J. Chen, *Chem. Soc. Rev.*, 2022, **51**, 1846–1860.
69 J. Song, C. Wei, Z.-F. Huang, C. Liu, L. Zeng, X. Wang and Z. J. Xu, *Chem. Soc. Rev.*, 2020, **49**, 2196–2214.

70 J. Zhang, C. Si, T. Kou, J. Wang and Z. Zhang, *Sustainable Energy Fuels*, 2020, **4**, 2625–2637.
71 Z. Chen, S. Yun, L. Wu, J. Zhang, X. Shi, W. Wei, Y. Liu, R. Zheng, N. Han and B.-J. Ni, *Nano-Micro Lett.*, 2023, **15**, 1–37.
72 X. Li, H. Wang, Z. Cui, Y. Li, S. Xin, J. Zhou, Y. Long, C. Jin and J. B. Goodenough, *Sci. Adv.*, 2019, **5**, eaav6262.
73 H. Ku, Y. Jung, M. Jo, S. Park, S. Kim, D. Yang, K. Rhee and E.-M. An, *J. Hazard. Mater.*, 2016, **313**, 138–146.
74 V. Pegoretti, P. Dixini, L. Magnago, A. Rocha, M. Lelis and M. Freitas, *Mater. Res. Bull.*, 2019, **110**, 97–101.
75 Y. Yang, C. R. Peltier, R. Zeng, R. Schimmenti, Q. Li, X. Huang, Z. Yan, G. Potsi, R. Selhorst and X. Lu, *Chem. Rev.*, 2022, **122**, 6117–6321.
76 C. Huang, H. Lv, Z. Yang, C. Lian, J. Du, G. Liu, W. Tang, Z. Xu, Z. Chi and H. Liu, *J. Mater. Chem. A*, 2022, **10**, 3359–3372.
77 H. Bian, W. Wu, Y. Zhu, C. H. Tsang, Y. Cao, J. Xu, X. Liao, Z. Lu, X.-Y. Lu and C. Liu, *ACS Sustainable Chem. Eng.*, 2023, **11**, 670–678.
78 B. Cui, C. Liu, J. Zhang, J. Lu, S. Liu, F. Chen, W. Zhou, G. Qian, Z. Wang and Y. Deng, *Sci. China Mater.*, 2021, **64**, 2710–2718.
79 Z. Chen, W. Zou, R. Zheng, W. Wei, W. Wei, B.-J. Ni and H. Chen, *Green Chem.*, 2021, **23**, 6538–6547.
80 H. Lv, H. Huang, C. Huang, Q. Gao, Z. Yang and W. Zhang, *Appl. Catal., B*, 2021, **283**, 119634.
81 R. Farzana, M. A. Sayeed, J. Joseph, K. Ostrikov, A. P. O'Mullane and V. Sahajwalla, *ChemElectroChem*, 2020, **7**, 2073–2080.
82 Y. Sun, X. L. Shi, Y. L. Yang, G. Suo, L. Zhang, S. Lu and Z. G. Chen, *Adv. Funct. Mater.*, 2022, **32**, 2201584.
83 H. Zhong, M. Wang, G. Chen, R. Dong and X. Feng, *ACS Nano*, 2022, **16**, 1759–1780.
84 C. Hu and L. Dai, *Adv. Mater.*, 2019, **31**, 1804672.
85 M. Fan, J. Cui, J. Wu, R. Vajtai, D. Sun and P. M. Ajayan, *Small*, 2020, **16**, 1906782.
86 Y. Li, Y. Qu, C. Liu, J. Cui, K. Xu, Y. Li, H. Shen, Z. Lu, H. Pan and T. Xu, *Adv. Sustainable Syst.*, 2022, **6**, 2100343.
87 R. Lu, D. K. Sam, W. Wang, S. Gong, J. Liu, A. Durairaj, M. Li and X. Lv, *J. Colloid Interface Sci.*, 2022, **613**, 126–135.
88 Y. Feng, Y. Guan, E. Zhou, X. Zhang and Y. Wang, *Adv. Sci.*, 2022, **9**, 2201339.
89 B. Zhang, Y. Zheng, T. Ma, C. Yang, Y. Peng, Z. Zhou, M. Zhou, S. Li, Y. Wang and C. Cheng, *Adv. Mater.*, 2021, **33**, 2006042.
90 X. Pei, S. Yi, Y. Zhao, Y. Mu, Y. Yu, M. Cui, C. Meng, C. Huang and Y. Zhang, *J. Colloid Interface Sci.*, 2022, **616**, 476–487.
91 A. Bähr, H. Petersen and H. Tüysüz, *ChemCatChem*, 2021, **13**, 3824–3835.
92 M. A. Ahsan, M. A. Imam, A. R. P. Santiago, A. Rodriguez, B. Alvarado-Tenorio, R. Bernal, R. Luque and J. C. Noveron, *Green Chem.*, 2020, **22**, 6967–6980.
93 H. A. Bandal, A. A. Pawar and H. Kim, *Electrochim. Acta*, 2022, **422**, 140545.
94 Z. Zhu and Z. Xu, *Renewable Sustainable Energy Rev.*, 2020, **134**, 110308.
95 X. Min, T. Zhang, M. Xie, K. Zhang, L. Chai, Z. Lin, C. Ding and Y. Shi, *ChemElectroChem*, 2022, **9**, e202200394.
96 P. E. Karthik, H. Rajan, V. R. Jothi, B.-I. Sang and S. C. Yi, *J. Hazard. Mater.*, 2022, **421**, 126687.
97 H. Zhou, Y. Ren, Z. Li, M. Xu, Y. Wang, R. Ge, X. Kong, L. Zheng and H. Duan, *Nat. Commun.*, 2021, **12**, 1–9.
98 M. A. Khan, M. T. Mehran, S. R. Naqvi, A. H. Khoja, F. Shahzad, U. Sikander, S. Hussain, R. Khan, B. Sarfaraz and M. M. Baig, *ACS Omega*, 2021, **6**, 21316–21326.
99 C. Sathiskumar, L. Meesala, P. Kumar, B. R. Rao, N. S. John and H. R. Matte, *Sustainable Energy Fuels*, 2021, **5**, 1406–1414.
100 A. K. Awasthi and J. Li, *Trends Biotechnol.*, 2019, **37**, 677–680.
101 E. Luo, Y. Chu, J. Liu, Z. Shi, S. Zhu, L. Gong, J. Ge, C. H. Choi, C. Liu and W. Xing, *Energy Environ. Sci.*, 2021, **14**, 2158–2185.
102 S. Yang, Y. Yu, X. Gao, Z. Zhang and F. Wang, *Chem. Soc. Rev.*, 2021, **50**, 12985–13011.
103 S. K. Singh, K. Takeyasu and J. Nakamura, *Adv. Mater.*, 2019, **31**, 1804297.
104 A. Kulkarni, S. Siahrostami, A. Patel and J. K. Nørskov, *Chem. Rev.*, 2018, **118**, 2302–2312.
105 Y. Li, K. Xiao, C. Huang, J. Wang, M. Gao, A. Hu, Q. Tang, B. Fan, Y. Xu and X. Chen, *Nano-Micro Lett.*, 2021, **13**, 1–14.
106 M. Muhyuddin, P. Mustarelli and C. Santoro, *ChemSusChem*, 2021, **14**, 3785–3800.
107 J. Zhu, W. Li, S. Li, J. Zhang, H. Zhou, C. Zhang, J. Zhang and S. Mu, *Small*, 2018, **14**, 1800563.
108 M. N. Jackson and Y. Surendranath, *Acc. Chem. Res.*, 2019, **52**, 3432–3441.
109 K. Liivand, M. Kazemi, P. Walke, V. Mikli, M. Uibu, D. D. Macdonald and I. Kruusenberg, *ChemSusChem*, 2021, **14**, 1103–1111.
110 M. Jiao, Q. Zhang, C. Ye, R. Gao, L. Dai, G. Zhou and H.-M. Cheng, *ACS Nano*, 2022, **16**, 13223–13231.
111 K. S. Bejigo, S. Natarajan, K. Bhunia, V. Elumalai and S.-J. Kim, *J. Cleaner Prod.*, 2023, **384**, 135520.
112 Y. Wang, M. Zhang, X. Shen, H. Wang, H. Wang, K. Xia, Z. Yin and Y. Zhang, *Small*, 2021, **17**, 2008079.
113 S. Xie, S. Huang, W. Wei, X. Yang, Y. Liu, X. Lu and Y. Tong, *ChemElectroChem*, 2015, **2**, 1806–1812.
114 Z. Xu, J. Ma, M. Shi, Y. Xie and C. Feng, *J. Colloid Interface Sci.*, 2018, **523**, 144–150.
115 V. Charles, X. Zhang, M. Yuan, K. Zhang, K. Cui, J. Zhang, T. Zhao, Y. Li, Z. Liu and B. Li, *Electrochim. Acta*, 2022, **402**, 139555.
116 K. Lee, Y. Jing, Y. Wang and N. Yan, *Nat. Rev. Chem.*, 2022, **6**, 635–652.
117 X. Zhao, B. Boruah, K. F. Chin, M. Đokić, J. M. Modak and H. S. Soo, *Adv. Mater.*, 2022, **34**, 2100843.

118 A. Veksha, J. G. S. Moo, V. Krikstolaityte, W.-D. Oh, W. C. Udayanga, A. Giannis and G. Lisak, *J. Electroanal. Chem.*, 2019, **849**, 113368.
119 N. Cai, H. Yang, X. Zhang, S. Xia, D. Yao, P. Bartocci, F. Fantozzi, Y. Chen, H. Chen and P. T. Williams, *Energy Convers. Manage.*, 2020, **109**, 119–126.
120 G. Daniel, T. Kosmala, M. C. Dalconi, L. Nodari, D. Badocco, P. Pastore, A. Lorenzetti, G. Granozzi and C. Durante, *Electrochim. Acta*, 2020, **362**, 137200.
121 J. Castelo-Quibén, E. Bailón-García, A. Moral-Rodríguez, F. Carrasco-Marín and A. F. Pérez-Cadenas, *Catal. Sci. Technol.*, 2022, **12**, 1187–1201.
122 W.-J. Liu, H. Jiang and H.-Q. Yu, *Energy Environ. Sci.*, 2019, **12**, 1751–1779.
123 H. Xie, T. Wang, J. Liang, Q. Li and S. Sun, *Nano Today*, 2018, **21**, 41–54.
124 F. Liang, K. Zhang, L. Zhang, Y. Zhang, Y. Lei and X. Sun, *Small*, 2021, **17**, 2100323.
125 J. Wu, S. Ma, J. Sun, J. I. Gold, C. Tiwary, B. Kim, L. Zhu, N. Chopra, I. N. Odeh and R. Vajtai, *Nat. Commun.*, 2016, **7**, 1–6.
126 D. Raciti and C. Wang, *ACS Energy Lett.*, 2018, **3**, 1545–1556.
127 S. Stojkovikj, G. A. El-Nagar, F. Firschke, L. C. Pardo Pérez, L. Choubrac, M. Najdoski and M. T. Mayer, *ACS Appl. Mater. Interfaces*, 2021, **13**, 38161–38169.
128 N. Sharma, A. Bajpai, P. K. Yadav, S. Nellaiappan, S. Sharma, C. S. Tiwary and K. Biswas, *ACS Sustainable Chem. Eng.*, 2020, **8**, 12142–12150.
129 T. Möller, W. Ju, A. Bagger, X. Wang, F. Luo, T. N. Thanh, A. S. Varela, J. Rossmeisl and P. Strasser, *Energy Environ. Sci.*, 2019, **12**, 640–647.
130 H. Han, S. Jin, S. Park, M. H. Seo and W. B. Kim, *Appl. Catal., B*, 2021, **292**, 120173.
131 P. Yao, Y. Qiu, T. Zhang, P. Su, X. Li and H. Zhang, *ACS Sustainable Chem. Eng.*, 2019, **7**, 5249–5255.
132 H. Wang, M. Li, G. Liu, L. Yang, P. Sun and S. Sun, *New J. Chem.*, 2021, **45**, 1063–1071.
133 R. S. Costa, B. S. Aranha, A. Ghosh, A. O. Lobo, E. T. da Silva, D. C. Alves and B. C. Viana, *J. Phys. Chem. Solids*, 2020, **147**, 109678.
134 W. Wang, L. Shang, G. Chang, C. Yan, R. Shi, Y. Zhao, G. I. Waterhouse, D. Yang and T. Zhang, *Adv. Mater.*, 2019, **31**, 1808276.
135 Z. Qin, X. Jiang, Y. Cao, S. Dong, F. Wang, L. Feng, Y. Chen and Y. Guo, *Sci. Total Environ.*, 2021, **759**, 143575.
136 R. Kanega, N. Onishi, L. Wang and Y. Himeda, *ACS Catal.*, 2018, **8**, 11296–11301.
137 Z. Huang, M. Rafiq, A. R. Woldu, Q.-X. Tong, D. Astruc and L. Hu, *Coord. Chem. Rev.*, 2023, **478**, 214981.
138 G.-F. Chen, Y. Yuan, H. Jiang, S.-Y. Ren, L.-X. Ding, L. Ma, T. Wu, J. Lu and H. Wang, *Nat. Energy*, 2020, **5**, 605–613.
139 H. Jiang, G. Chen, O. Savateev, J. Xue, L.-X. Ding, Z. Liang, M. Antonietti and H. Wang, *Angew. Chem., Int. Ed.*, 2023, **62**, e202218717.
140 L. Hu, Z. Xing and X. Feng, *ACS Energy Lett.*, 2020, **5**, 430–436.
141 Y. Ren, C. Yu, X. Tan, H. Huang, Q. Wei and J. Qiu, *Energy Environ. Sci.*, 2021, **14**, 1176–1193.
142 L. Deng, L. Wang, G. Wei, H. Yuan, J. Xie and Y. Chen, *Electrochim. Acta*, 2022, **408**, 139934.
143 Y. Zhang, Y. Cui, J. Zhang, Y. Xu, Q. Liu and G. Qian, *Chem. Eng. J.*, 2022, **429**, 132357.
144 G. F. Chen, A. Savateev, Z. Song, H. Wu, Y. Markushyna, L. Zhang, H. Wang and M. Antonietti, *Angew. Chem., Int. Ed.*, 2022, **61**, e202203170.
145 B. H. Suryanto, K. Matuszek, J. Choi, R. Y. Hodgetts, H.-L. Du, J. M. Bakker, C. S. Kang, P. V. Cherepanov, A. N. Simonov and D. R. MacFarlane, *Science*, 2021, **372**, 1187–1191.
146 Z. Zhu, T. Jiang, M. Ali, Y. Meng, Y. Jin, Y. Cui and W. Chen, *Chem. Rev.*, 2022, **122**, 16610–16751.
147 J. Pu, Z. Shen, C. Zhong, Q. Zhou, J. Liu, J. Zhu and H. Zhang, *Adv. Mater.*, 2020, **32**, 1903808.
148 C. M. Costa, J. C. Barbosa, R. Gonçalves, H. F. Castro, F. J. d. Campo and S. Lanceros-Méndez, *Energy Storage Mater.*, 2021, **37**, 433–465.
149 P. Daubinger, M. Schelter, R. Petersohn, F. Nagler, S. Hartmann, M. Herrmann and G. A. Giffin, *Adv. Energy Mater.*, 2022, **12**, 2102448.
150 M. R. Palacín, *Chem. Soc. Rev.*, 2018, **47**, 4924–4933.
151 S. Gantenbein, M. Schönleber, M. Weiss and E. Ivers-Tiffée, *Sustainability*, 2019, **11**, 6697.
152 X. Li, S. Liu, J. Yang, Z. He, J.-c. Zheng and Y. Li, *Energy Storage Mater.*, 2022, **55**, 606–630.
153 X. Zhang, Y. Bian, S. Xu, E. Fan, Q. Xue, Y. Guan, F. Wu, L. Li and R. Chen, *ACS Sustainable Chem. Eng.*, 2018, **6**, 5959–5968.
154 B. Gangaja, S. Nair and D. Santhanagopalan, *ACS Sustainable Chem. Eng.*, 2021, **9**, 4711–4721.
155 J. Zhu, G. Guo, J. Wu, X. Cheng and Y. Cheng, *Ionics*, 2022, **28**, 241–250.
156 C. Yuwen, B. Liu, H. Zhang, S. Tian, L. Zhang, S. Guo and B. Zhou, *J. Cleaner Prod.*, 2022, **333**, 130197.
157 Y. Xiao, J. Li, W. Huang, L. Wang and J. Luo, *J. Mater. Sci.: Mater. Electron.*, 2022, **33**, 16740–16752.
158 D. Ruan, L. Wu, F. Wang, K. Du, Z. Zhang, K. Zou, X. Wu and G. Hu, *J. Electroanal. Chem.*, 2021, **884**, 115073.
159 X. Zhu, J. Xiao, Q. Mao, Z. Zhang, Z. You, L. Tang and Q. Zhong, *Chem. Eng. J.*, 2022, **430**, 132703.
160 X. Zhu, J. Xiao, Y. Chen, L. Tang, H. Hou, Z. Yao, Z. Zhang and Q. Zhong, *Chem. Eng. J.*, 2022, **450**, 138113.
161 Z. Chen, A. Soltani, Y. Chen, Q. Zhang, A. Davoodi, S. Hosseinpour, W. Peukert and W. Liu, *Adv. Energy Mater.*, 2022, **12**, 2200924.
162 P. Li, H. Kim, S.-T. Myung and Y.-K. Sun, *Energy Storage Mater.*, 2021, **35**, 550–576.
163 J. Cao, Y. Sim, X. Y. Tan, J. Zheng, S. W. Chien, N. Jia, K. Chen, Y. B. Tay, J. F. Dong and L. Yang, *Adv. Mater.*, 2022, **34**, 2110518.

164 W. Kang, J.-C. Kim and D.-W. Kim, *J. Power Sources*, 2020, **468**, 228407.
165 W. Zhang, D. Wang, H. Shi, H. Jiang, C. Wang, X. Niu, L. Yu, X. Zhang, Z. Ji and X. Yan, *Sustainable Mater. Technol.*, 2022, **33**, e00454.
166 J. Lu, J. Liu, X. Gong, S. j. Pang, C.-y. Zhou, H. Li, G. Qian and Z. Wang, *Energy Storage Mater.*, 2022, **46**, 594–604.
167 C. Wang, X. Niu, D. Wang, W. Zhang, H. Shi, L. Yu, C. Wang, Z. Xiong, Z. Ji, X. Yan and Y. Gu, *Powder Technol.*, 2022, **408**, 117744.
168 Y. Feng, L. Tao, Z. Zheng, H. Huang and F. Lin, *Energy Storage Mater.*, 2020, **31**, 274–309.
169 Q. Feng, H. Li, Z. Tan, Z. Huang, L. Jiang, H. Zhou, H. Pan, Q. Zhou, S. Ma and Y. Kuang, *Adv. Energy Mater.*, 2018, **6**, 19479–19487.
170 J. E. Entwistle, S. G. Booth, D. S. Keeble, F. Ayub, M. Yan, S. A. Corr, D. J. Cumming and S. V. Patwardhan, *Adv. Energy Mater.*, 2020, **10**, 2001826.
171 A. Su, J. Li, J. Dong, D. Yang, G. Chen and Y. Wei, *Small*, 2020, **16**, 2001714.
172 C. Senthil, K. Vediappan, M. Nanthagopal, H. S. Kang, P. Santhoshkumar, R. Gnanamuthu and C. W. Lee, *Chem. Eng. J.*, 2019, **372**, 765–773.
173 C. Zhang, Q. Jiang, A. Liu, K. Wu, Y. Yang, J. Lu, Y. Cheng and H. Wang, *Carbohydr. Polym.*, 2020, **237**, 116134.
174 J. Lu, Y. Wang, F. Song, Z. Zhang, Q. Lu, Y. Cheng, Y. Tao, J. Du and H. Wang, *J. Power Sources*, 2022, **531**, 231318.
175 J. Balach, J. Linnemann, T. Jaumann and L. Giebeler, *J. Mater. Chem. A*, 2018, **6**, 23127–23168.
176 Z. Wang, X. Zhang, X. Liu, Y. Zhang, W. Zhao, Y. Li, C. Qin and Z. Bakenov, *J. Colloid Interface Sci.*, 2020, **569**, 22–33.
177 Y. Hu, W. Chen, T. Lei, Y. Jiao, J. Huang, A. Hu, C. Gong, C. Yan, X. Wang and J. Xiong, *Adv. Energy Mater.*, 2020, **10**, 2000082.
178 P. Liu, Y. Wang and J. Liu, *J. Energy Chem.*, 2019, **34**, 171–185.
179 K. Wang, J.-B. Le, S.-J. Zhang, W.-F. Ren, J.-M. Yuan, T.-T. Su, B.-Y. Chi, C.-Y. Shao and R.-C. Sun, *J. Mater. Chem. A*, 2022, **10**, 4845–4857.
180 C. Jin, O. Sheng, W. Zhang, J. Luo, H. Yuan, T. Yang, H. Huang, Y. Gan, Y. Xia, C. Liang, J. Zhang and X. Tao, *Energy Storage Mater.*, 2018, **15**, 218–225.
181 A. Benítez, J. Amaro-Gahete, Y.-C. Chien, Á. Caballero, J. Morales and D. Brandell, *Renewable Sustainable Energy Rev.*, 2022, **154**, 111783.
182 Y. Kim, Y. Noh, J. Bae, H. Ahn, M. Kim and W. B. Kim, *J. Energy Chem.*, 2021, **57**, 10–18.
183 Y. Xie, J. Cao, X. Wang, W. Li, L. Deng, S. Ma, H. Zhang, C. Guan and W. Huang, *Nano Lett.*, 2021, **21**, 8579–8586.
184 Q. Xiao, G. Li, M. Li, R. Liu, H.-b. Li, P. Ren, Y. Dong, M. Feng and Z. Chen, *J. Energy Chem.*, 2020, **44**, 61–67.
185 X. Wu, L. Fan, M. Wang, J. Cheng, H. Wu, B. Guan, N. Zhang and K. Sun, *ACS Appl. Mater. Interfaces*, 2017, **9**, 18889–18896.
186 R. Khatoon, S. Attique, R. Liu, S. Rauf, N. Ali, L. Zhang, Y.-J. Zeng, Y. Guo, Y. V. Kaneti and J. Na, *Green Energy Environ.*, 2022, **7**, 1071–1083.
187 X. Yang, R. Li, J. Yang, H. Liu, T. Luo, X. Wang and L. Yang, *Carbon*, 2022, **199**, 215–223.
188 P. Półrolniczak, D. Kasprzak, J. Kaźmierczak-Raźna, M. Walkowiak, P. Nowicki and R. Pietrzak, *Synth. Met.*, 2020, **261**, 116305.
189 K. Song, D. A. Agyeman, M. Park, J. Yang and Y. M. Kang, *Adv. Mater.*, 2017, **29**, 1606572.
190 D. Wang, X. Mu, P. He and H. Zhou, *Mater. Today*, 2019, **26**, 87–99.
191 Y. M. Wang and Y. C. Lu, *Energy Storage Mater.*, 2020, **28**, 235–246.
192 Z. Sun, H. Wang, J. Wang and T. Zhang, *Energy Storage Mater.*, 2019, **23**, 670–677.
193 D. Li, Q. Wang, Y. Yao, F. Wu, Y. Yu and C. Zhang, *ACS Appl. Mater. Interfaces*, 2018, **10**, 32058–32066.
194 M. Wang, Y. Yao, Z. Tang, T. Zhao, F. Wu, Y. Yang and Q. Huang, *ACS Appl. Mater. Interfaces*, 2018, **10**, 32212–32219.
195 X. Zhu, Y. Shang, Y. Lu, C. Liu, Z. Li and Q. Liu, *J. Power Sources*, 2020, **471**, 228444.
196 I. Izanzar, M. Dahbi, M. Kiso, S. Doubaji, S. Komaba and I. Saadoune, *Carbon*, 2019, **146**, 844.
197 R. Muruganantham, T.-H. Hsieh, C.-H. Lin and W.-R. Liu, *Mater. Today Energy*, 2019, **14**, 100346.
198 A. F. Qatarneh, C. Dupont, J. Michel, L. Simonin, A. Beda, C. M. Ghimbeu, V. Ruiz-Villanueva, D. da Silva, H. Piégay and M. J. Franca, *J. Environ. Chem. Eng.*, 2021, **9**, 106604.
199 R. Muruganantham, F.-M. Wang and W.-R. Liu, *Electrochim. Acta*, 2022, **424**, 140573.
200 S. Rubio, T. Odoom-Wubah, Q. Li, J. L. Tirado, P. Lavela, J. Huang and G. F. Ortiz, *J. Cleaner Prod.*, 2022, **359**, 131994.
201 Q. Deng, H. Liu, Y. Zhou, Z. Luo, Y. Wang, Z. Zhao and R. Yang, *J. Electroanal. Chem.*, 2021, **899**, 115668.
202 W. Cao, E. Zhang, J. Wang, Z. Liu, J. Ge, X. Yu, H. Yang and B. Lu, *Electrochim. Acta*, 2019, **293**, 364–370.
203 C. Gao, Q. Wang, S. Luo, Z. Wang, Y. Zhang, Y. Liu, A. Hao and R. Guo, *J. Power Sources*, 2019, **415**, 165–171.
204 Z. Yi, G. Chen, F. Hou, L. Wang and J. Liang, *Adv. Energy Mater.*, 2021, **11**, 2170001.
205 Z. Chen, J. Hu, T. He, C. Feng, Y. Luo, H. Hou, G. Zou and X. Ji, *Energy Storage Mater.*, 2022, **50**, 1–11.
206 M. Jiao, Q. Zhang, C. Ye, Z. Liu, X. Zhong, J. Wang, C. Li, L. Dai, G. Zhou and H. M. Cheng, *PANS*, 2022, **119**, e2202202119.
207 X. Li, J. Zhang, B. Liu and Z. Su, *J. Cleaner Prod.*, 2021, **310**, 127428.
208 N. Choudhary, C. Li, J. Moore, N. Nagaiah, L. Zhai, Y. Jung and J. Thomas, *Adv. Mater.*, 2017, **29**, 1605336.
209 H. Abdolpour, P. Niewiadomski and Ł. Sadowski, *Constr. Build. Mater.*, 2021, **309**, 125147.

210 S. Natarajan, K. Krishnamoorthy, A. Sathyaseelan, V. K. Mariappan, P. Pazhamalai, S. Manoharan and S.-J. Kim, *Nano Energy*, 2022, **101**, 107595.
211 E. Barbieri, E. Lima, M. Lelis and M. Freitas, *J. Power Sources*, 2014, **270**, 158–165.
212 X. Sun, C. Huang, L. Wang, L. Liang, Y. Cheng, W. Fei and Y. Li, *Adv. Mater.*, 2021, **33**, 2001105.
213 X. Duan, J. Deng, X. Wang and P. Liu, *Mater. Des.*, 2017, **129**, 135–142.
214 S. Natarajan, K. Krishnamoorthy and S.-J. Kim, *J. Hazard. Mater.*, 2022, **430**, 128496.
215 K. K. Jena, A. T. Mayyas, B. Mohanty, B. K. Jena, J. R. Jos, A. AlFantazi, B. Chakraborty and A. A. Almarzooqi, *Energy Fuels*, 2022, **36**, 2159–2170.
216 S. Long, Y. Feng, F. He, J. Zhao, T. Bai, H. Lin, W. Cai, C. Mao, Y. Chen and L. Gan, *Nano Energy*, 2021, **85**, 105973.
217 W. Zhang, J. Yin, C. Wang, L. Zhao, W. Jian, K. Lu, H. Lin, X. Qiu and H. N. Alshareef, *Small Methods*, 2021, **5**, 2100896.
218 J. Wang, P. Nie, B. Ding, S. Dong, X. Hao, H. Dou and X. Zhang, *J. Mater. Chem. A*, 2017, **5**, 2411–2428.
219 C. Fang, P. Hu, S. Dong, Y. Cheng, D. Zhang and X. Zhang, *J. Colloid Interface Sci.*, 2021, **582**, 552–560.
220 Y. Li, S. Liu, Y. Liang, Y. Xiao, H. Dong, M. Zheng, H. Hu and Y. Liu, *ACS Sustainable Chem. Eng.*, 2019, **7**, 13827–13835.
221 H. Xu, L. Wang, Y. Zhang, Y. Chen and S. Gao, *Nanoscale*, 2021, **13**, 10051–10060.
222 L.-H. Zheng, M.-H. Chen, S.-X. Liang and Q.-F. Lü, *Diamond Relat. Mater.*, 2021, **113**, 108267.
223 K. Subhani, X. Jin, N. Hameed, J. Ramshaw, V. Glattauer and N. Salim, *Mater. Today Sustain.*, 2022, **18**, 100152.
224 G. Nagaraju, S. C. Sekhar and J. S. Yu, *Adv. Energy Mater.*, 2018, **8**, 1702201.
225 J. A. Bennett, K. Wilson and A. F. Lee, *J. Mater. Chem. A*, 2016, **4**, 3617–3637.
226 K. Krishnamoorthy, M. Sudhakaran, P. Pazhamalai, V. K. Mariappan, Y. S. Mok and S.-J. Kim, *J. Mater. Chem. A*, 2019, **7**, 18950–18958.
227 J. Lim, J. Hwang and J. H. Byeon, *Green Chem.*, 2019, **21**, 491–497.
228 H. Zhang, X.-L. Zhou, L.-M. Shao, F. Lü and P.-J. He, *Sci. Total Environ.*, 2021, **772**, 145309.
229 C. Ma, J. Min, J. Gong, X. Liu, X. Mu, X. Chen and T. Tang, *Chemosphere*, 2020, **253**, 126755.
230 Y. Li, D. Zhang, J. He, Y. Wang, X. Zhang, Y. Zhang, X. Liu, K. Wang and Y. Wang, *Sustainable Energy Fuels*, 2019, **3**, 499–507.
231 S. Kaipannan, P. A. Ganesh, K. Manickavasakam, S. Sundaramoorthy, K. Govindarajan, S. Mayavan and S. Marappan, *J. Energy Storage*, 2020, **32**, 101774.

